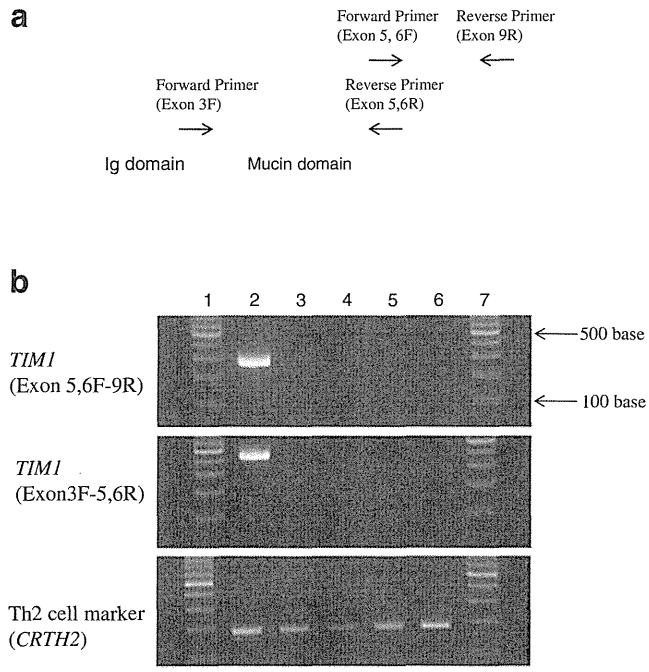

Fig. 2 Expression of *TIM1* in T cell lines. **a** TIM1 cDNA is schematically shown. *Arrows* indicate the regions of PCR primers which were designed in the highly conserved coding regions of *TIM1* among human and New World monkeys. **b** From *left* to *right*: *lane 1* 100-bp ladder size marker, *lane 2* Jurkat (human), *lane 3* HSF-10 (tufted capuchin), *lane 4* HSQ-115 (common squirrel monkey), *lane 5* HST-3 (white-lipped tamarin), *lane 6* HSCj-109 (common marmoset), and *lane 7* 100-bp ladder size marker. A marker gene (*CRTH2*) was used as a positive control of gene expression because it is known to be expressed in T cells especially in Th2-type cells

than the ds values in several lineages, especially in the Old World monkeys (Fig. 1). Sequence alignment of TIM1 at the amino acid (AA) level in the primates is shown in Fig. 3. To identify possible target sites for positive selection, we analyzed the TIM1 sequences by the BEB method. Sixteen TIM1 sequences from primate species, human, chimpanzee, bonobo, western gorilla, Bornean orangutan, western black-crested gibbon, lar gibbon, siamang, rhesus macaque, long-tailed macaque, Hamadryas baboon, mantled Guereza colobus, dusky leaf monkey, silver leaf monkey, white-fronted spider monkey, and Sunda slow loris, were used in the statistical test. It was revealed that 14 AA sites, at 23, 25, 30, 37, 51, 54, 58, 59, 72, 93, 102,120, 125, and 288 positions equivalent to the human TIM1, were the positively selected sites. These 14 AA sites were highly variable among the 16 primate sequences, e.g., AA site at 23 was lysine in hominoid; asparagine in rhesus macaque, long-tailed macaque, Hamadryas baboon, and mantled Guereza colobus; tyrosine in dusky leaf monkey and silver leaf monkey; serine in white-fronted spider monkey; and glutamine in Sunda slow loris. Most of the positive selection sites (10/14: 71.4 %) were found in the Ig domain (Fig. 3a, b).

Diversity of TIM1 in the Old World monkey

As shown in Fig. 3, a large number of deletion/insertion events were observed in the mucin domain (Fig. 3b, c). It was reported that human TIM1 exhibited a high degree of amino-acid variability in the mucin domain (Nakajima et al. 2005). Because the mucin domain of TIM1 encoded by exon 4 might be under the positive selection in the Old World monkey (Supplemental Table S4), we investigated the diversity of TIM1 in rhesus macaques by determining nucleotide sequences for the mucin domain from eight samples (16 haplotypes). As shown in Fig. 4, a high level of sequence diversity with multiple insertion/deletion of 18-bp sequences, A(T/C)GACAAC(G/A)(A/G)C(T/C)CT(T/G)CCA forming a part of AA stretch Thr-Thr-Thr-Thr-Leu-Pro (TTTTLP), was observed in the mucin domain of rhesus TIM1. We then investigated a possible selection by using the Bn-Bs program, but no statistically significant data were obtained, presumably because the compared sequences were not long enough to give a definite conclusion. However, when we calculated Tajima's *D* for these *TIM1* alleles, a value of 0.607 was obtained, which suggested a balanced selection of polymorphisms in the mucin domain of TIM1 in the Old World monkey.

On the other hand, because the diversity of mucin domain in the rhesus macaques could be detectable as a length diversity of exon 4, we examined length variations of *TIM1* exon 4 in additional samples of rhesus and long-tailed macaques. It was found that the length polymorphism was due to the repeat number polymorphisms or insertion/deletion polymorphisms of 18-bp unit and its components of 3- and 6-bp repeats (Supplemental Table S5).

Discussion

In this study, we investigated sequence diversity in the protein coding exons of *TIM1* from various species by direct sequencing method. Although there were a few sites with heterozygous sequences, we used "evolutionary conserved" sequences obtained from each sample in the statistical analyses so that the substitutions were underestimated in this study. Even though there was an underestimation, we demonstrated that the Ig domain of TIM1 has been under the positive selection during the course of primate evolution. Another interesting finding was that TIM1 has undergone pseudogene evolution in the New World monkey. It was suggested that the generation of pseudogene had occurred several times over the New World monkey lineages, by the insertion of deleterious sequences or base substitutions leading to a termination codon. Similar natural selection pattern was reported for type 1 vomeronasal receptors (*VIRL*), in which the pseudogene generation had independently

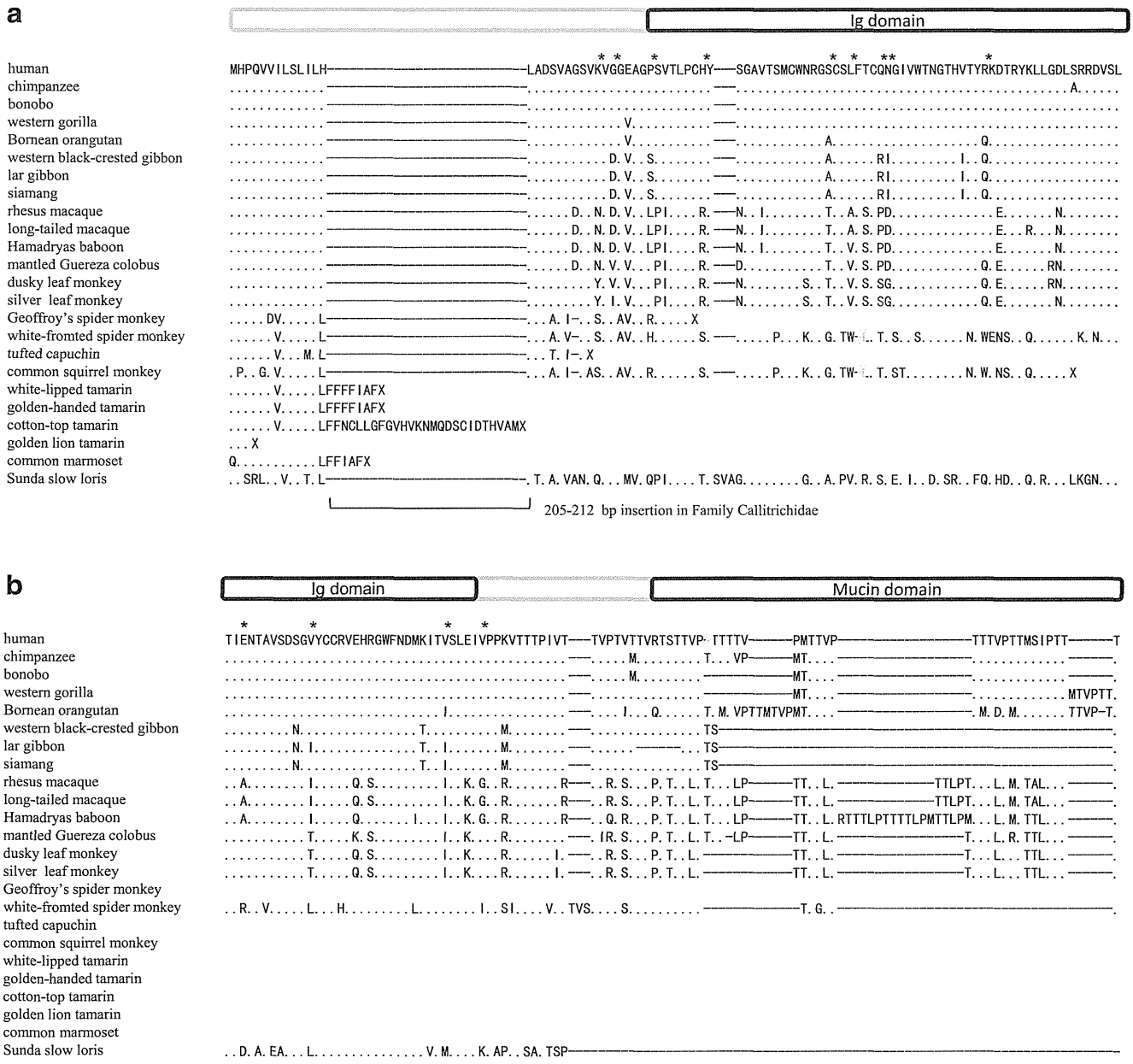

Fig. 3 Alignments of TIM1 amino acid sequences from 24 primate species. *Dots* indicate identities to the human reference sequence, while *dashes* indicate alignment gaps. *Asterisks* indicate AA sites identified as being under the significant positive selection ($p<0.05$). **a**, **b**, **c**, and **d** represent quarter parts of TIM1 from N-terminus to C-terminus. Ig and mucin domains are schematically indicated

occurred in the human and other primate lineages, implying that the function of *V1RL* might be highly lineage specific (Mundy and Cook 2003).

TIM1 plays an important role in generation and/or maintenance of the balance between Th1 and Th2 cells (Su et al. 2008). It is known that a natural ligand for TIM1 is T-cell Ig domain and mucin domain containing protein 4 (TIM4) (Meyers et al. 2005a), and the interaction of TIM1 with TIM4 plays a crucial role in sustaining the polarization status of Th2 cells (Khademi et al. 2004; Mariat et al. 2005). Because TIM1 expressed on the surface of Th2 cells regulated the immune response by modulating cytokine production in mammals, the Th1/Th2 balance might be skewed or affected by the lack of TIM1 in the most lineages of New World monkey. Previous study demonstrated that expression of Th1-type cytokines, IFN-γ and TNF-β, was considerably lower than that of Th2-type cytokines, IL-4 and IL-10, in a New World monkey, owl monkey (Pico de Coana et al. 2004). This observation may support the disturbance of Th1/Th2 balance in the owl monkey lacking TIM1, although we cannot exclude a possibility that some other molecules than TIM1 might regulate Th1/Th2 balance

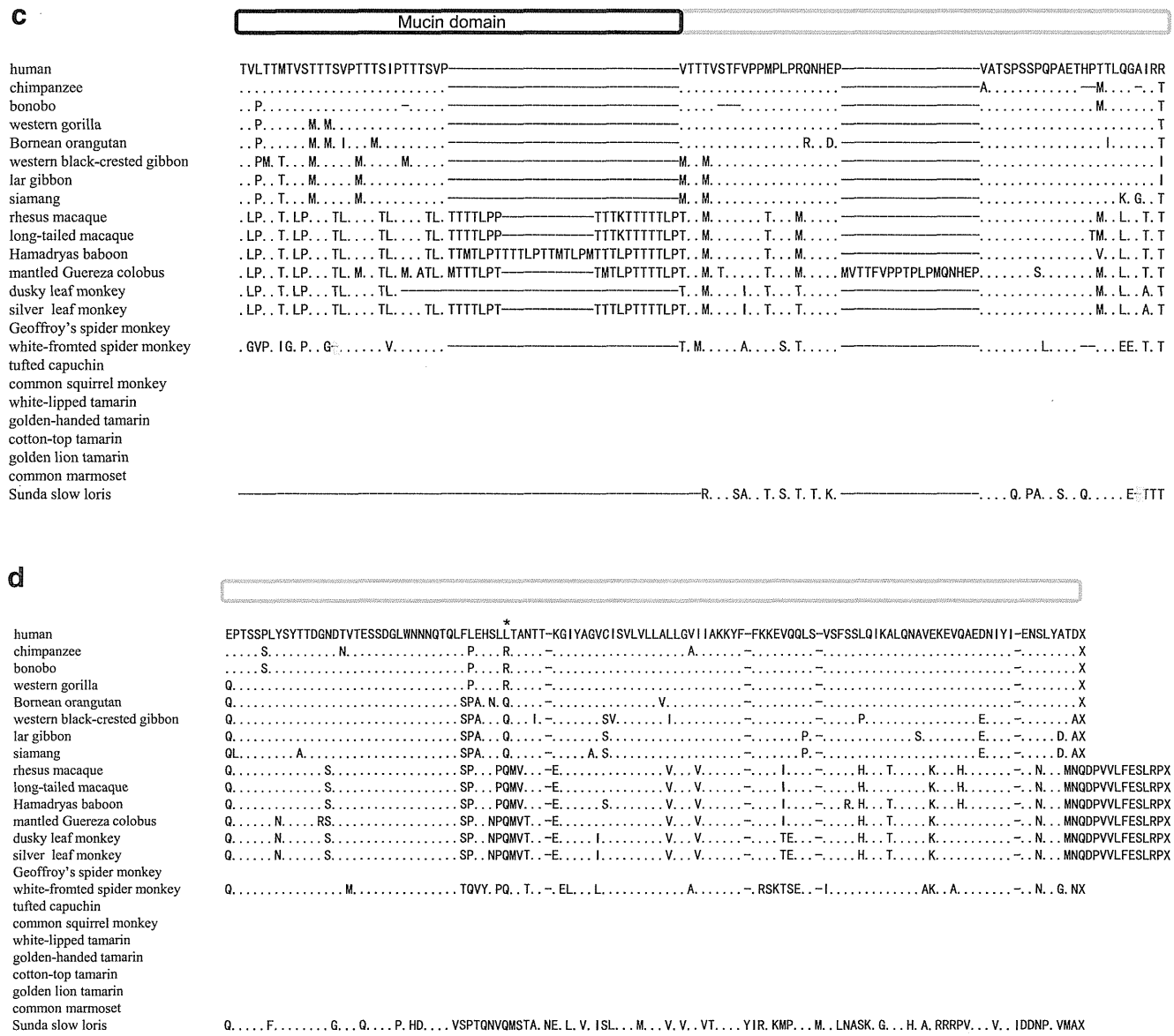

Fig. 3 (continued)

in the primates including the TIM1-deficient New World monkey. It is interesting to note that there is a *TIM1*-like gene on chromosome 13 in the marmoset genome, which might replace the function of *TIM1*. However, this TIM1-like gene lacks introns and contains several in-frame stop codons, when it is aligned with human *TIM1* (Supplemental Figure S2).

It is known that TIM1 is a cellular receptor for hepatitis A virus (HAV) in human (Feigelstock et al. 1998). The results in this study suggested that the New World monkey lineages

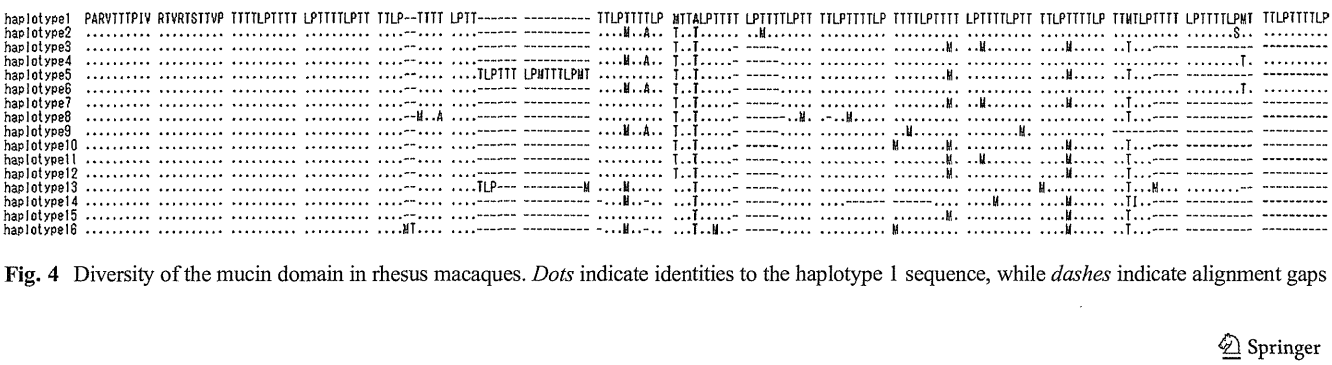

Fig. 4 Diversity of the mucin domain in rhesus macaques. *Dots* indicate identities to the haplotype 1 sequence, while *dashes* indicate alignment gaps

might lack a cellular receptor for HAV, TIM1. However, because the New World monkey is susceptible to HAV infection (Mathiesen et al. 1980), further studies are needed to clarify or find other cellular receptors for HAV in the New World monkey and a cause or reason of pseudogene generation, which had occurred in several lineages of the New World monkey. In addition, it has been reported that TIM1 polymorphisms are associated with resistance to autoimmune diseases including multiple sclerosis, which are associated with the imbalance between Th1 and Th2 cells (Khademi et al. 2004). Nevertheless, common marmosets are used as an animal model for multiple sclerosis, experimental autoimmune encephalomyelitis (Uccelli et al. 2003). Thus, susceptibilities of the New World monkey to the autoimmune diseases should be investigated in relation to the non-functional TIM1.

In this study, 14 AA sites of TIM1 were identified as positively selected sites in the evolutional course of primates other than the New World monkey. It was suggested that the Ig domain of TIM1 was a binding site for HAV (Feigelstock et al. 1998). In addition, structural conformation of the mucin domain is required for the efficient viral entry (McIntire et al. 2003). In this study, TIM1 was considered to be under the significant positive natural selection in the Ig domain, prompting us to investigate the three dimensional (3D) structures of the Ig domains using SWISS-MODEL, an Automated Comparative Protein Modeling Server (http://swissmodel.expasy.org/SWISS-MODEL.html) (Bordoli et al. 2009). As shown in Fig. 5, it was suggested that most of the target sites for the positive selection accumulated on the surface of Ig domain. These observations support a hypothesis that the evolution of TIM1 in the primates might be driven by exogenous pathogens. The positively selected sites in the Ig domain of TIM1 in the primates other than the New World monkey and a high level diversity in the mucin domain of TIM1 in the Old World monkey might be a direct consequence of a selection pressure exerted by HAV. However, because TIM1 polymorphisms are also associated with other infectious diseases including HIV/AIDS and cerebral malaria, further functional studies are required to clarify the mechanism of natural selection at specific sites of Ig and mucin domains of TIM1. For example, we are now investigating whether the TIM1 repeat polymorphism would influence the production level of neutralizing antibodies against challenging Simian Immunodeficiency Virus (SIV) in experimental models of SIV vaccination in rhesus macaques (Sugimoto et al. 2010; Ishii et al. 2012; Nomura et al. 2012).

Because TIM1 is known to interact with TIM4 and both Ig and mucin domains of TIM1 are involved in this interaction (Meyers et al. 2005a), one might speculate a co-evolution of TIM1 and TIM4. It should be noted here that human TIM family includes three members, TIM1, TIM3, and TIM4, while mouse TIM family includes eight members, TIM1 toTIM8. Although we searched for orthologs of mouse TIM2, TIM5, TIM6, TIM7, and TIM8 in the common marmoset genome by using Blat program (http://genome.ucsc.edu/cgi-bin/hgBlat), we could not detect any orthologous genes. Therefore, TIM family in the New World monkey consists of only two functional members, TIM3 and TIM4. Then, we investigated a possible evolutionary selection of TIM3 and TIM4. However, no significant positive selection appeared to operate on the evolution of TIM3 and TIM4 in the primates (Supplemental Table S6). A marginal and non-significant positive selection for TIM4 in chimpanzee was observed, but it may not correlate with co-evolution of TIM1 and TIM4, because the mucin domain of TIM1 is virtually non-polymorphic in chimpanzee (Nakajima et al. 2005). Nevertheless, the observations in this study suggest that the diversity of TIM family is widely ranged among mammalian species. It may be of interest to investigate whether the binding affinity of TIM1 and TIM4 would be affected by the TIM1 variations in future experiments. On the other hand, it may be noteworthy that TIM1, TIM3, and TIM4 can independently serve as receptors for phosphatidylserine to mediate uptake of apoptotic cells (Kobayashi et al. 2007; Freeman et al. 2010), implying that their cooperation would be dispensable in some functional aspects.

In conclusion, we investigated the molecular evolution of TIM1 in 24 primate species. TIM1 had become pseudogenes in most lineages of the New World monkey, while it

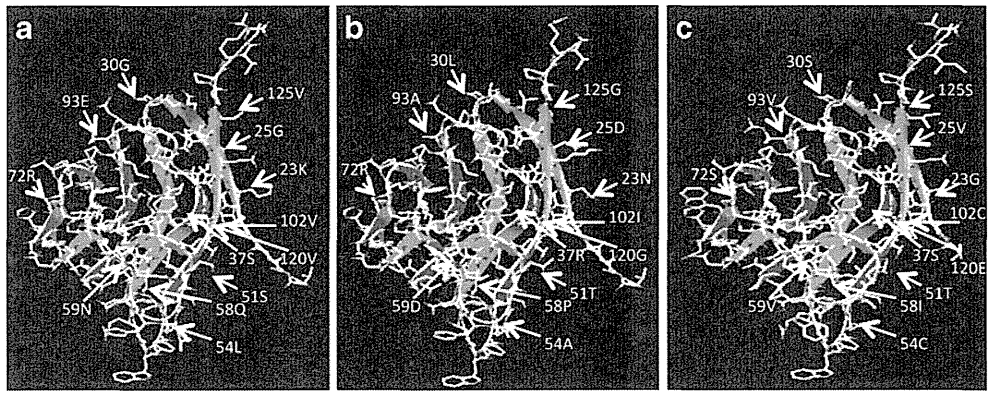

Fig. 5 Three-dimensional structures of TIM1 modeled by SWISS-MODEL. *Arrows* indicate AA sites identified as being under the positive selection by using the BEB method in the PAML program. **a** human TIM1, **b** rhesus macaque TIM1, **c** long-haired spider monkey TIM1

was under the positive selection in the other primates, especially in the Old World monkey. TIM1 might undergo a selection pressure exerted by infectious disease and autoimmune disease.

Acknowledgments We would like to thank Dr. Toshiaki Nakajima for his critical comments and contributions in the initial course of this study. This work was supported in part by research grants from the Ministry of Health, Labor and Welfare, Japan; by Grant-in-Aids for scientific research from the Ministry of Education, Culture, Sports, Science, and Technology (MEXT), Japan; by grants for India–Japan Cooperative Science Program from Japan Society for the Promotion of Science (JSPS), Japan and Department of Science and Technology (DST), India; and Joint Usage/Research Programs of Research Institute for Microbial Diseases, Osaka University and Medical Research Institute Tokyo Medical and Dental University. This work was also supported by a program of support for women researchers from the Tokyo Medical and Dental University.

References

Barreiro LB, Quintana-Murci L (2010) From evolutionary genetics to human immunology: how selection shapes host defence genes. Nat Rev Genet 11:17–30

Bordoli L, Kiefer F, Arnold K, Benkert P, Battey J, Schwede T (2009) Protein structure homology modeling using SWISS-MODEL workspace. Nat Protoc 4:1–13

Chatterjee HJ, Ho SY, Barnes I, Groves C (2009) Estimating the phylogeny and divergence times of primates using a supermatrix approach. BMC Evol Biol 9:259

de Souza AJ, Kane LP (2006) Immune regulation by the TIM gene family. Immunol Res 36:147–155

Feigelstock D, Thompson P, Mattoo P, Zhang Y, Kaplan GG (1998) The human homolog of HAVcr-1 codes for a hepatitis A virus cellular receptor. J Virol 72:6621–6628

Freeman GJ, Casasnovas JM, Umetsu DT, DeKruyff RH (2010) TIM genes: a family of cell surface phosphatidylserine receptors that regulate innate and adaptive immunity. Immunol Rev 235:172–189

Gibbs RA et al (2007) Evolutionary and biomedical insights from the rhesus macaque genome. Science 316:222–234

Hohjoh H, Akari H, Fujiwara Y, Tamura Y, Hirai H, Wada K (2009) Molecular cloning and characterization of the common marmoset huntingtin gene. Gene 432:60–66

Hollox EJ, Armour JA (2008) Directional and balancing selection in human beta-defensins. BMC Evol Biol 8:113

Ichimura T, Bonventre JV, Bailly V, Wei H, Hession CA, Cate RL, Sanicola M (1998) Kidney injury molecule-1 (KIM-1), a putative epithelial cell adhesion molecule containing a novel immunoglobulin domain, is up-regulated in renal cells after injury. J Biol Chem 273:4135–4142

Ishii H, Kawada M, Tsukamoto T, Yamamoto H, Matsuoka S, Shiino T, Takeda A, Inoue M, Iida A, Hara H, Shu T, Hasegawa M, Naruse TK, Kimura A, Takiguchi M, Matano T (2012) Impact of vaccination on cytotoxic T lymphocyte immunodominance and cooperation against simian immunodeficiency virus replication in rhesus macaques. J Virol 86:738–745

Khademi M, Illes Z, Gielen AW, Marta M, Takazawa N, Baecher-Allan C, Brundin L, Hannerz J, Martin C, Harris RA, Hafler DA, Kuchroo VK, Olsson T, Piehl F, Wallstrom E (2004) T cell Ig- and mucin-domain-containing molecule-3 (TIM-3) and TIM-1 molecules are differentially expressed on human Th1 and Th2 cells and in cerebrospinal fluid-derived mononuclear cells in multiple sclerosis. J Immunol 172:7169–7176

Kobayashi N, Karisola P, Peña-Cruz V, Dorfman DM, Jinushi M, Umetsu SE, Butte MJ, Nagumo H, Chernova I, Zhu B, Sharpe AH, Ito S, Dranoff G, Kaplan GG, Casasnovas JM, Umetsu DT, Dekruyff RH, Freeman GJ (2007) TIM-1 and TIM-4 glycoproteins bind phosphatidylserine and mediate uptake of apoptotic cells. Immunity 27:927–940

Kosiol C, Vinar T, da Fonseca RR, Hubisz MJ, Bustamante CD, Nielsen R, Siepel A (2008) Patterns of positive selection in six mammalian genomes. PLoS Genet 4:e1000144

Kuchroo VK, Umetsu DT, DeKruyff RH, Freeman GJ (2003) The TIM gene family: emerging roles in immunity and disease. Nat Rev Immunol 3:454–462

Mariat C, Sanchez-Fueyo A, Alexopoulos SP, Kenny J, Strom TB, Zheng XX (2005) Regulation of T cell dependent immune responses by TIM family members. Philos Trans R Soc Lond B Biol Sci 360:1681–1685

Mathiesen LR, Moller AM, Purcell RH, London WT, Feinstone SM (1980) Hepatitis A virus in the liver and intestine of marmosets after oral inoculation. Infect Immun 28:45–48

McIntire JJ, Umetsu SE, Macaubas C, Hoyte EG, Cinnioglu C, Cavalli-Sforza LL, Barsh GS, Hallmayer JF, Underhill PA, Risch NJ, Freeman GJ, DeKruyff RH, Umetsu DT (2003) Immunology: hepatitis A virus link to atopic disease. Nature 425:576

McIntire JJ, Umetsu DT, DeKruyff RH (2004) TIM-1, a novel allergy and asthma susceptibility gene. Springer Semin Immunopathol 25:335–348

Meyers JH, Chakravarti S, Schlesinger D, Illes Z, Waldner H, Umetsu SE, Kenny J, Zheng XX, Umetsu DT, DeKruyff RH, Strom TB, Kuchroo VK (2005a) TIM-4 is the ligand for TIM-1, and the TIM-1-TIM-4 interaction regulates T cell proliferation. Nat Immunol 6:455–464

Meyers JH, Sabatos CA, Chakravarti S, Kuchroo VK (2005b) The TIM gene family regulates autoimmune and allergic diseases. Trends Mol Med 11:362–369

Mundy NI, Cook S (2003) Positive selection during the diversification of class I vomeronasal receptor-like (V1RL) genes, putative pheromone receptor genes, in human and primate evolution. Mol Biol Evol 20:1805–1810

Nakajima T, Wooding S, Satta Y, Jinnai N, Goto S, Hayasaka I, Saitou N, Guan-Jun J, Tokunaga K, Jorde LB, Emi M, Inoue I (2005) Evidence for natural selection in the HAVCR1 gene: high degree of amino-acid variability in the mucin domain of human HAVCR1 protein. Genes Immun 6:398–406

Nei M, Gojobori T (1986) Simple methods for estimating the numbers of synonymous and nonsynonymous nucleotide substitutions. Mol Biol Evol 3:418–426

Nomura T, Terahara K, Yamamoto H, Shiino T, Takahashi N, Nakane T, Iwamoto N, Ishii H, Tsukamoto T, Kawada M, Matsuoka S, Takeda A, Terahara K, Tsunetsugu-Yokota Y, Iwata-Yoshikawa N, Hasegawa H, Sata T, Naruse TK, Kimura A, Matano T (2012) Association of major histocompatibility complex class I haplotypes with disease progression after simian immunodeficiency virus challenge in Burmese rhesus macaques. J Virol 86:6481–6490

Ohtani H, Nakajima T, Akari H, Ishida T, Kimura A (2011) Molecular evolution of immunoglobulin superfamily genes in primates. Immunogenetics 63:417–418

Pico de Coana Y, Barrero C, Cajiao I, Mosquera C, Patarroyo ME, Patarroyo MA (2004) Quantifying Aotus monkey cytokines by real-time quantitative RT-PCR. Cytokine 27:129–133

Rzhetsky A, Nei M (1993) Theoretical foundation of the minimum-evolution method of phylogenetic inference. Mol Biol Evol 10:1073–1095

Sawyer SL, Emerman M, Malik HS (2004) Ancient adaptive evolution of the primate antiviral DNA-editing enzyme APOBEC3G. PLoS Biol 2:E275

Su EW, Lin JY, Kane LP (2008) TIM-1 and TIM-3 proteins in immune regulation. Cytokine 44:9–13

Sugimoto C, Watanabe S, Naruse T, Kajiwara E, Shiino T, Umano N, Ueda K, Sato H, Ohgimoto S, Hirsh V, Villinger F, Ansari AA, Kimura A, Miyazawa M, Suzuki Y, Yamamoto N, Nagai Y, Mori K (2010) Protection of macaques with diverse MHC genotypes against a heterologous SIV by vaccination with a deglycosylated live-attenuated SIV. PLoS One 5:e11678

Tajima F (1989) Statistical method for testing the neutral mutation hypothesis by DNA polymorphism. Genetics 123:585–595

Tamura K, Peterson D, Peterson N, Stecher G, Nei M, Kumar S (2011) Molecular evolutionary genetics analysis using maximum likelihood, evolutionary distance, and maximum parsimony methods. Mol Biol Evol 28(10):2731–2739

Uccelli A, Giunti D, Capello E, Roccatagliata L, Mancardi GL (2003) EAE in the common marmoset *Callithrix jacchus*. Int MS J 10:6–12

Wichukchinda N, Nakajima T, Saipradit N, Nakayama EE, Ohtani H, Rojanawiwat A, Pathipvanich P, Ariyoshi K, Sawanpanyalert P, Shioda T, Kimura A (2010) TIM1 haplotype may control the disease progression to AIDS in a HIV-1-infected female cohort in Thailand. AIDS 24:1625–1631

Wong WS, Yang Z, Goldman N, Nielsen R (2004) Accuracy and power of statistical methods for detecting adaptive evolution in protein coding sequences and for identifying positively selected sites. Genetics 168:1041–1051

Yang Z (2005) The power of phylogenetic comparison in revealing protein function. Proc Natl Acad Sci U S A 102:3179–3180

Yang Z, Nielsen R (2000) Estimating synonymous and nonsynonymous substitution rates under realistic evolutionary models. Mol Biol Evol 17:32–43

Yang Z, Wong WS, Nielsen R (2005) Bayes empirical Bayes inference of amino acid sites under positive selection. Mol Biol Evol 22:1107–1118

Zhang J, Rosenberg HF, Nei M (1998) Positive Darwinian selection after gene duplication in primate ribonuclease genes. Proc Natl Acad Sci U S A 95:3708–3713

JVI Journals.ASM.org

A Noncanonical mu-1A-Binding Motif in the N Terminus of HIV-1 Nef Determines Its Ability To Downregulate Major Histocompatibility Complex Class I in T Lymphocytes

Sayuki Iijima,[a,b] Young-Jung Lee,[a] Hirotaka Ode,[d] Stefan T. Arold,[c] Nobuyuki Kimura,[a] Masaru Yokoyama,[d] Hironori Sato,[d] Yasuhito Tanaka,[b] Klaus Strebel,[e] and Hirofumi Akari[a,f]

Laboratory of Disease Control, Tsukuba Primate Research Center, National Institute of Biomedical Innovation, Hachimandai, Tsukuba-shi, Ibaraki, Japan[a]; Department of Virology, Liver Unit, Nagoya City University Graduate School of Medical Sciences, Kawasumi, Mizuho, Nagoya, Japan[b]; Department of Biochemistry and Molecular Biology, MD Anderson Cancer Center, Houston, Texas, USA[c]; Pathogen Genomics Center, National Institute of Infectious Diseases, Gakuen, Musashimurayama, Tokyo, Japan[d]; Laboratory of Molecular Microbiology, National Institute of Allergy and Infectious Diseases, NIH, Bethesda, Maryland, USA[e]; and Primate Research Institute, Kyoto University, Inuyama, Aichi, Japan[f]

Downregulation of major histocompatibility complex class I (MHC-I) by HIV-1 Nef protein is indispensable for evasion of protective immunity by HIV-1. Though it has been suggested that the N-terminal region of Nef contributes to the function by associating with a mu-1A subunit of adaptor protein 1, the structural basis of the interaction between Nef and mu-1A remains elusive. We found that a tripartite hydrophobic motif (Trp13/Val16/Met20) in the N terminus of Nef was required for the MHC-I downregulation. Importantly, the motif functioned as a noncanonical mu-1A-binding motif for the interaction with the tyrosine motif-binding site of the mu-1A subunit. Our findings will help understanding of how HIV-1 evades the antiviral immune response by selectively redirecting the cellular protein trafficking system.

Nef is an *N*-myristoylated protein of 27 to 35 kDa conserved among primate lentiviruses, and the expression of human immunodeficiency virus type 1 (HIV-1) Nef contributes to the progression of AIDS (4). One of the multiple functions of Nef is the downregulation of major histocompatibility complex class I (MHC-I) (41). MHC-I downregulation by Nef has been shown to protect infected cells from cytotoxic T lymphocyte (CTL) killing (9, 36, 44, 50), contributing to viral persistence *in vivo* (44). However, the molecular mechanism by which Nef downregulates MHC-I is not fully understood.

Previous reports have shown that several functional residues in Nef contribute to MHC-I downregulation. For instance, deletion of N-terminal residues 17 to 26 abolishes the Nef function (27). In particular, Met20 was found to be indispensable for MHC-1 downmodulation (2). In addition, residues 62 to 65 of Nef are critical for the ability of Nef to target MHC-I (37, 39). The residues reportedly function as a binding site for phosphofurin acidic cluster sorting protein 1 (PACS-1) (10), although this conclusion is still controversial (5, 24). Finally, the $_{69}$-PxxP-$_{78}$ region in the core domain, which is associated with its ligand molecules having an SH3 domain, is required for the function (17). Nef does not affect MHC-I synthesis and transport to the endoplasmic reticulum and the *cis* Golgi apparatus (41); hence, Nef is thought to act on MHC-1 as it traffics from the trans-Golgi network (TGN) to the plasma membrane or in the recycling pathway. The mu-1A subunit of adapter protein complex 1 (AP-1) has been shown to act as an essential factor in MHC-I downregulation (23, 40), and hypothetical models that involve complexes of Nef, mu-1A, and MHC-I have been proposed (29, 49). However, the structural basis for Nef interaction with mu-1A remains to be elucidated. In this study, we further examined the role of Met 20 in the N terminus of Nef and found that a conserved tripartite hydrophobic motif composed of Trp13 and Val16 as well as Met20 acted as a novel motif for the interaction with the tyrosine motif-binding site of the mu-1A subunit.

MATERIALS AND METHODS

Plasmid constructs. The plasmids encoding HIV-1 proviral genomes containing *nef* gene mutants were designed based on pNL4-3 (1). The Nef(−), M20A, M20R (2), Δmyr, R mutant (48), and Δ62-68 mutant (39) were described previously. The mutant Nef(−) lacks expression of Nef because of an alteration of the first ATG codon to ACC. Met20 was replaced with Ala and Arg for M20A and M20R, respectively. Δmyr lacks the signal for myristoylation by Glu-to-Ala substitution. The R mutant replaced four instances of Arg at residues 17, 19, 21, and 22 with Ala. Δ62-68 deleted residues 62 to 67.

To generate substitution mutants, we digested *env*-defective variant pNL43-K1 (7) with BamHI and XhoI, and the fragment encoding a portion of the *nef* gene was subcloned into pGEM-7zf (Promega, Japan). Based on this subcloning plasmid, we generated substitution mutants by site-directed mutagenesis using *Pfu* Turbo DNA polymerase (Stratagene, La Jolla, CA) and the following primers: for G12A, 5′-GGTCAAAGAGT AGTGTGATTGCGTGGCCAGCTG-3′ and 5′-CAGCTGGCCACGCAA TCACACTACTCTTTGACC-3′; for G12E, 5′-GGTCAAAGAGTAGTGT GATTGAGTGGCCAGCTG-3′ and 5′-CAGCTGGCCACTCAATCACA CTACTCTTTGACC-3′; for G12R, 5′-GGTCAAAGAGTAGTGTGATTC GCTGGCCAGCTG-3′ and 5′-CAGCTGGCCAGCGAATCACACTACT CTTTGACC-3′; for W13A, 5′-GTGATTGGCGCCCCTGCTGTAAGGG AAAG-3′ and 5′-CTTTCCCTTACAGCAGGGGCGCCAATCAC-3′; for W13Y, 5′-GTAGTGTGATTGGATATCCTGCTGTAAGGGAAAG-3′ and 5′-CTTTCCCTTACAGCAGGATATCCAATCACGCTGC-3′; for V16A, 5′-GTGATTGGATGGCCAGCTGCGAGGGAAAGAATGAG-3′ and 5′-CTCATTCTTTCCCTCGCAGCTGGCCATCCAATCAC-3′; for V16E, 5′-GTGATTGGATGGCCAGCTGAGAGGGAAAGAATGAG-3′ and 5′-CTCATTCTTTCCCTCTCAGCTGGCCATCCAATCAC-3′; for

Received 8 September 2011 Accepted 18 January 2012
Published ahead of print 1 February 2012
Address correspondence to Hirofumi Akari, akari@pri.kyoto-u.ac.jp.

doi:10.1128/JVI.06257-11

V16R, 5′-GTGATTGGATGGCCAGCTCGGAGGGAAAGAATGAG-3′ and 5′-CTCATTCTTTCCCTCCGAGCTGGCCATCCAATCAC-3′; for E18A, 5′-GATTGGATGGCCAGCTGTAAGGGCCAGAATGAG-3′ and 5′-CTCATTCTGGCCCTTACAGCTGGCCATCCAATC-3′; for E18D, 5′-GATTGGATGGCCAGCTGTAAGGGACAGAATGAG-3′ and 5′-CTCATTCTGTCCCTTACAGCTGGCCATCCAATC-3′; and for E18R, 5′-GATTGGATGGCCAGCTGTAAGGCGGAGAATGAG-3′ and 5′-CTCATTCTCCGCCTTACAGCTGGCCCATCCAATC-3′.

All constructs described above were verified by nucleotide sequencing with a BigDye Terminator cycle sequencing kit (version 1.1) and a Genetic Analyzer (ABI PRISM 3100; Applied Biosystems, Foster City, CA). The A-MLV-Env expression plasmid SA-A-MLV vector (34) and the VSV-G expression construct pCMV-G (51) were used for the production of pseudotyped viruses by cotransfection with pNL4-3 or its variants as previously described (3).

Cell culture. 293T cells were cultured in Dulbecco's modified Eagle's medium with 5% fetal bovine serum (Sigma-Aldrich, St. Louis, MO) and antibiotics. CEM-GFP cells contain HIV-1 long-terminal-repeat-driven green fluorescence protein (GFP) cDNA, and GFP expression is inducible by Tat (14). The cells and Jurkat cells were maintained with RPMI 1640 with 10% fetal bovine serum and antibiotics.

Antibodies. In this study, we used the following antibodies: a rabbit polyclonal anti-Nef antibody (2949) and an AIDS-patient serum (provided by the AIDS Research and Reference Reagent Program, NIH), an RPE-cy5-conjugated or a nonlabeled anti-CD4 monoclonal antibody (MAb) (MT310; Dako, Japan), anti-HLA-ABC MAbs (B9.12.1, Beckman Coulter, Fullerton, CA; W6/32, ebioscience, San Diego, CA), an allophycocyanin (APC)-conjugated goat anti-mouse Ig (BD Bioscience, San Jose, CA), an anti-gamma-adaptin MAb (100/3; Sigma), an anti-NeuN MAb (A60; Millipore, Hercules, CA), and a rabbit anti-mu-1A antibody (Sigma) (28).

Transfection and preparation of viruses, cell lysates, and viral lysates and Western blotting. 293T cells were transfected with pNL4-3 or its *nef* mutants by the use of Lipofectamine 2000 (Invitrogen, San Diego, CA). Transfected 293T cells (2×10^7) and culture supernatants were harvested at 48 h posttransfection. The culture supernatants were filtered (0.45-μm-pore-size filter), quantified for p24 capsid antigen levels by enzyme-linked immunosorbent assay (ELISA) (ZeptoMetrix, Buffalo, NY), and stored at −80°C. The cells were washed with phosphate-buffered saline (PBS) twice and resuspended in PBS with protease inhibitor cocktails (Complete Mini; Roche, Mannheim, Germany) and lysed with 2× sample buffer for 5 min at 95°C. For harvesting viral particles, the virus supernatants were ultracentrifuged through a cushion of 20% (wt/vol) sucrose–PBS at 110,000 × *g* for 60 min at 4°C and then lysed with 2× sample buffer for 5 min at 95°C. The protocol of Western blotting was based on a previously described method (3). To detect the Nef and p24 proteins in cell lysates and viral particles, we used anti-Nef polyclonal antibody and AIDS-patient serum, respectively. Immunoreactive proteins were visualized using chemiluminescence (Immobilon; Millipore).

Downregulation assay. CEM-GFP cells (5×10^5) were infected with viruses by spinoculation at 30°C and 1,200 × *g* for 2 h as previously described (30). The cells were immediately transferred to the T25 flask with fresh medium and cultured at 37°C. At 48 h after infection, the cells were incubated with an RPE-cy5-conjugated anti-CD4 MAb or an anti-HLA-ABC MAb, followed by treatment with an APC-conjugated anti-mouse Ig at 4°C for 30 min. The fluorescence intensity for GFP and MHC-I was detected by a FACSCalibur flow cytometer (BD Bioscience).

Immunofluorescence staining. At 24 h after infection, HIV-1-infected cells were transferred to chamber slides. Cells were incubated at 37°C for 30 min and centrifuged at 600 rpm for 5 min at room temperature. Cells were fixed with 3% paraformaldehyde at room temperature for 15 min, washed once with PBS, and incubated with a primary antibody solution overnight at 4°C. We subjected the following primary antibodies to double staining: an anti-CD4 MAb (MT310) (1:1,000), an anti-HLA-ABC MAb (W6/32) (1:5,000), and an anti-Nef polyclonal antibody (1:5,000). After one wash with PBS, cells were incubated with an Alexa 555-conjugated anti-rabbit IgG antibody or an Alexa 488-conjugated anti-mouse IgG antibody for 1 h at 4°C. After two washes with PBS and one wash with distilled water, we mounted samples on soft-mount solution (Wako). We subjected the following antibodies to triple staining: an anti-Nef MAb (1:500) labeled with a secondary antibody (Alexa 405) (1:500), stained using a Zenon labeling kit (Invitrogen); an anti-mu-1A polyclonal antibody (1:10,000); and an anti-HLA-ABC MAb (W6/32) (1:5,000). The samples were examined with a Digital Eclipse C1 confocal microscope (Nikon, Kanagawa, Japan).

Visualization of Nef N terminus based on the NMR model. Molecular structures were analyzed based on the nuclear magnetic resonance (NMR) model of the myristoylated Nef N terminus (Protein Data Bank [PDB] code 1QA5) (15). Structures were visualized using PyMol (W. L. DeLano; http://pymol.org), and hydrophobic accessible surface areas were calculated with Surface Racer (45).

Molecular modeling of the mu-1A subunit, the N-terminal region of Nef, and the complex of mu-1A with the N-terminal region of Nef. We constructed structural models of a human mu-1A protein with homology modeling, using two crystal structures of a rat AP-2 mu-2 subunit (PDB codes 1BW8 and 1HES) (32, 33) as the modeling templates, with the BioInfoBank Meta Server (http://meta.bioinfo.pl/). Homology modeling of mu-1A and structural models of the wild type (WT) and four mutants of the HIV-1 Nef N terminus (residues 9 to 26, with PDB code 1QA5 used as a modeling template) (15) was done using the SwissModel server (http://swissmodel.expasy.org/workspace/). The mu-1A model was subjected to docking with Nef N-terminal models by the use of a ASEDock module (Ryoka Systems Inc., Tokyo, Japan) (16) operated in the Molecular Operating Environment (MOE). The precision of docking results determined with the ASEDock module is generally equivalent to the experimental error value (i.e., a few angstroms); a result of dTTP docking with the ASEDock at the catalytic site in a reverse transcriptase (RT) closed configuration had a root-mean-square deviation of about 1.6 Å compared to that determined by X-ray crystallography (1RTD), which was a range within the resolution of the crystal structure (8). Potential sites of binding of mu-1A to the Nef peptides were searched with SiteFinder module and selected on the basis of analogy to the interaction between mu-2 and the YxxΦ motif (32, 33). Upon reviewing the results of the simulations, we considered the conformational flexibilities of peptide and side chains of mu-1A. Conformations of both main and side chains of the Nef peptides were randomly searched, and the Nef peptide models were automatically arranged in the binding cleft of mu-1A. Energy minimization of the peptide–mu-1A complex was performed under conditions in which the side chain atoms in mu-1A and all atoms in the peptide were not constrained but the main chain atoms in the mu-1A were tethered with 100 kcal/mol/Å^2. The AMBER ff99 force field (47) and the generalized Born/volume integral (GB/VI) implicit solvent model (22) were applied for the modeling. The three-dimensional (3D) structures were thermodynamically optimized by energy minimization using the MOE package and the same force field. A physically unacceptable local structure of the optimized 3D model was further assessed and refined on the basis of Ramachandran plot evaluation using the MOE package and 3D structure evaluation with Verify3D software (http://nihserver.mbi.ucla.edu/Verify_3D/) (26).

MD simulation. To estimate the binding affinity of a Nef N-terminal region to the mu-1A subunit, we performed molecular dynamics (MD) simulations and the subsequent binding energy calculations with AMBER 9 software (35). For the top-ranked model of the docking simulation of mu-1A and each Nef, a 1.5-ns (10^{-9} s) MD simulation was initiated at 300°K (26.85°C) with a time step of 1.0 fs (10^{-15} s). The AMBER ff99SB force field (19) and the GB implicit solvent model (IGB = 5) (31) were applied for potential energy calculations. The cutoff for long-distance-interaction energy was set at 15.0 Å, and the SHAKE algorithm was applied for bonds concerning hydrogen atoms. Subsequently, using 500 tra-

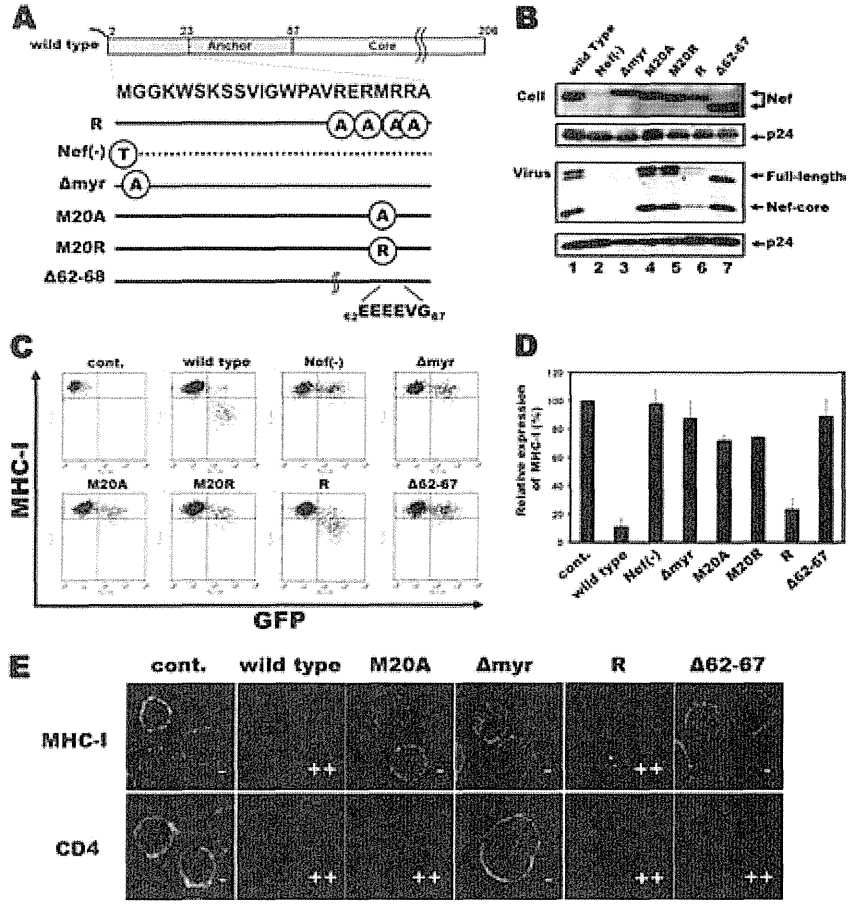

FIG 1 The basic cluster in the amino-terminal region did not contribute to the Nef function of MHC-I downregulation. (A) Schematic diagram of Nef mutants in the N-terminal region. Amino acid numbers are given above the box. The N-terminal myristoyl moiety is depicted as a zigzag line. (B) Detection of the cellular expression and viral packaging of WT and mutant Nef proteins. Upper panels, anti-Nef antibody; lower panels, AIDS-patient serum. (C) Analysis of the MHC-I downregulation by Nef mutants. CEM-GFP cells were infected with equal amounts of viruses. The cells were treated with an anti-HLA-ABC MAb, followed by staining with an APC-conjugated anti-mouse Ig. GFP-positive cells, i.e., HIV-1-infected cells, were analyzed for fluorescence intensity by flow cytometry. cont., uninfected cells. (D) The levels of MHC-I expression in the GFP-positive population. Data are shown as percentages of the MHC-I expression on the cell surface in comparison with the control as 100%. The ratios of all samples were calculated using the means of fluorescence intensity data. (E) Analysis of MHC-I and CD4 downregulation by immunofluorescence staining. At 48 h after infection, CEM-GFP cells were immunostained with MHC-I, CD4, and Nef antibodies. Green, MHC-I or CD4; red, Nef.

jectories during 1.0 to 1.5 simulations, we estimated approximated values of binding energy (ΔGb) between mu-1A and each Nef by the molecular mechanics/Poisson-Boltzmann surface area (MM/PBSA) method (21). The AMBER ff99SB force field and the PBSA methods (25) were applied for potential energy calculations. The PBSA method is more time-consuming but more accurate than the GB method. The cutoff value was applied for calculations of long-distance-interaction energy.

Coimmunoprecipitation. For immunoprecipitation, we used an anti-gamma-adaptin MAb, which was reported previously to coimmunoprecipitate the mu-1A subunit (11), or an anti-NeuN MAb, which expresses only in neural cells, as a negative control. At 20 h after HIV-1 infection, Jurkat cells were incubated with 20 mM NH_4Cl for 4 h. It was confirmed that this treatment did not influence the levels of MHC-I downregulation in the infected Jurkat cells. We harvested and lysed the cells with lysis buffer (1% digitonin, 150 mM NaCl, 50 mM Tris-HCl [pH 7.0], 1 mM $CaCl_2$, 1 mM $MgCl_2$, Complete Mini) for 20 min on ice. The lysates were centrifuged at 6,000 rpm for 1 min at 4°C, and the supernatants were recovered and precleared with 50 μl of Dynabeads (Invitrogen) for 1 h at 4°C. Also, 50 μl of beads and antibodies were mixed and incubated for 90 min at 4°C to form the bead-Ig complexes. The complexes were washed once with the lysis buffer, the precleared supernatant was added, and the mixture was incubated for 90 min at 4°C for immunoreactions. After the immunoreactions, the beads were washed 4 times with lysis buffer. The immunoprecipitated materials were eluted with 40 μl of 0.1% citrate at room temperature, 2× sample buffer was added, and the mixture was boiled for 5 min at 95°C. The samples were analyzed by Western blotting. Input controls were 1/50 of the volume of the immunoprecipitated protein. Consistent results were obtained from three independent experiments.

RESULTS

Analysis of the importance of the N-terminal region of Nef for MHC-I downregulation. A basic cluster (Arg17, -19, -21, and -22) is relatively conserved among Nef proteins of various HIV-1 subtypes. It has been shown that the basic cluster supports plasma membrane binding of myristoylated proteins by contributing electrostatic interactions with negatively charged acidic phospholipids such as phosphatidylserine and phosphatidylinositol at the cytosolic surface of the plasma membrane (38). We therefore hypothesized that Met20 and the basic cluster could cooperatively contribute to the MHC-I downregulation. To evaluate this possibility, we analyzed the function of a Nef variant referred to as the R mutant in which the Arg residues were replaced by Ala (Fig. 1A).

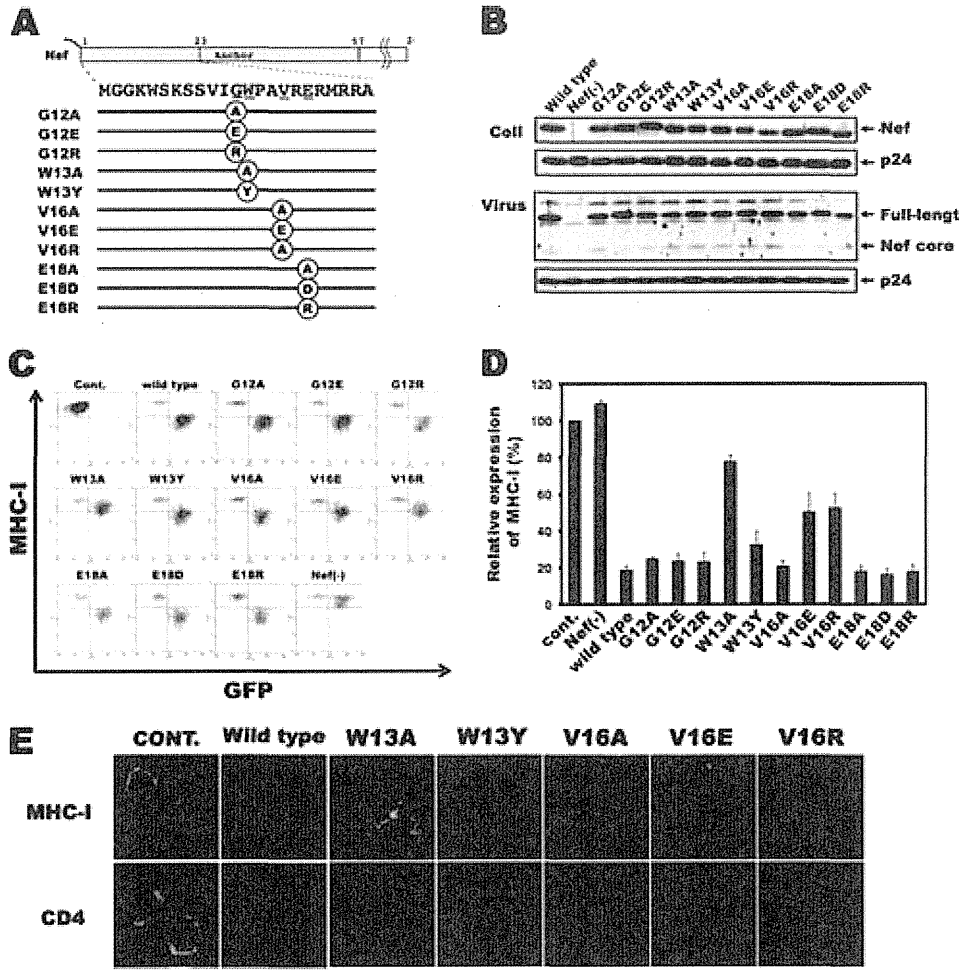

FIG 2 Conserved hydrophobic residues in the N terminus of Nef contribute to the function of MHC-I downregulation. (A) Schematic diagram of substitution mutants in the N terminus of Nef. Amino acid numbers are given above the box. (B) The cellular expression and viral packaging of WT Nef and Nef mutants. Nef and p24 CA protein were detected by Western blotting. (C) Flow cytometric analysis of the MHC-I downregulation by Nef. CEM-GFP cells were infected with the viruses as indicated and stained for MHC-1 at 48 h after infection as described for Fig. 1. Cont., uninfected cells. (D) The level of MHC-I expression in the GFP-positive subpopulation. Data shown are percentages of the MHC-I expression on the cell surface in comparison with the uninfected control (cont.) as 100%. The ratios of all samples were calculated as described in the Fig. 1D legend. (E) Analysis of MHC-I and CD4 localization by immunofluorescence staining. Green, MHC-I or CD4; red, Nef.

First, we determined the expression of Nef mutants and confirmed that WT Nef and its variants were intracellularly expressed at comparable levels. Virion packaging was less efficient in the R mutant (Fig. 1B), as previously shown (48). Next, we analyzed the effect of the mutations on the MHC-I downregulation. WT Nef clearly downregulated MHC-I on the surface of the HIV-1-infected T cells, while the Nef(−), M20A, M20R, and Δ62-68 variants lost the ability to downregulate MHC-I (Fig. 1C, D, and E). Contrary to our expectations, the R mutant retained an ability to downregulate MHC-I nearly equivalent to that of the WT (Fig. 1C, D, and E). In addition, the ability of the R mutant as well as the M20A, M20R, and Δ62-68 variants to downregulate CD4 was comparable to that seen with WT Nef (Fig. 1E). These results indicate that the reduced ability of the R mutant to incorporate into virions, which may be due to inefficient association with acidic phospholipids of the plasma membrane via electrostatic interactions as described previously (6), had no detectable effect on the MHC-I-regulatory function of Nef.

The N-terminal region of Nef has a number of conserved amino acid residues other than the basic cluster. It is conceivable that, in addition to Met20, they could cooperatively contribute to the Nef activity. In order to examine this possibility, we selected four residues as candidates, i.e., Gly12, Trp13, Val16, and Glu18, which are adjacent to Met20 and are relatively conserved among various HIV-1 subtypes. These residues were replaced with residues of a different electric charge or length of side chain (Fig. 2A). It was confirmed that the characteristics of expression as well as virion incorporation of these mutants were comparable (Fig. 2B). Interestingly, replacement of Trp13 by Ala but not by Tyr and of Val16 by Glu or Arg but not by Ala affected the Nef effect (Fig. 2C, D, and E). All these mutants were comparable to WT Nef in their ability to downregulate CD4 (Fig. 2E). Moreover, it was confirmed that double (W13A/V16R) and triple (W13A/V16R/M20A) substitution mutants of Nef also lost the ability to downregulate MHC-I but remained active with respect to CD4 (data not shown). Taken together, our data indicated that, in addition

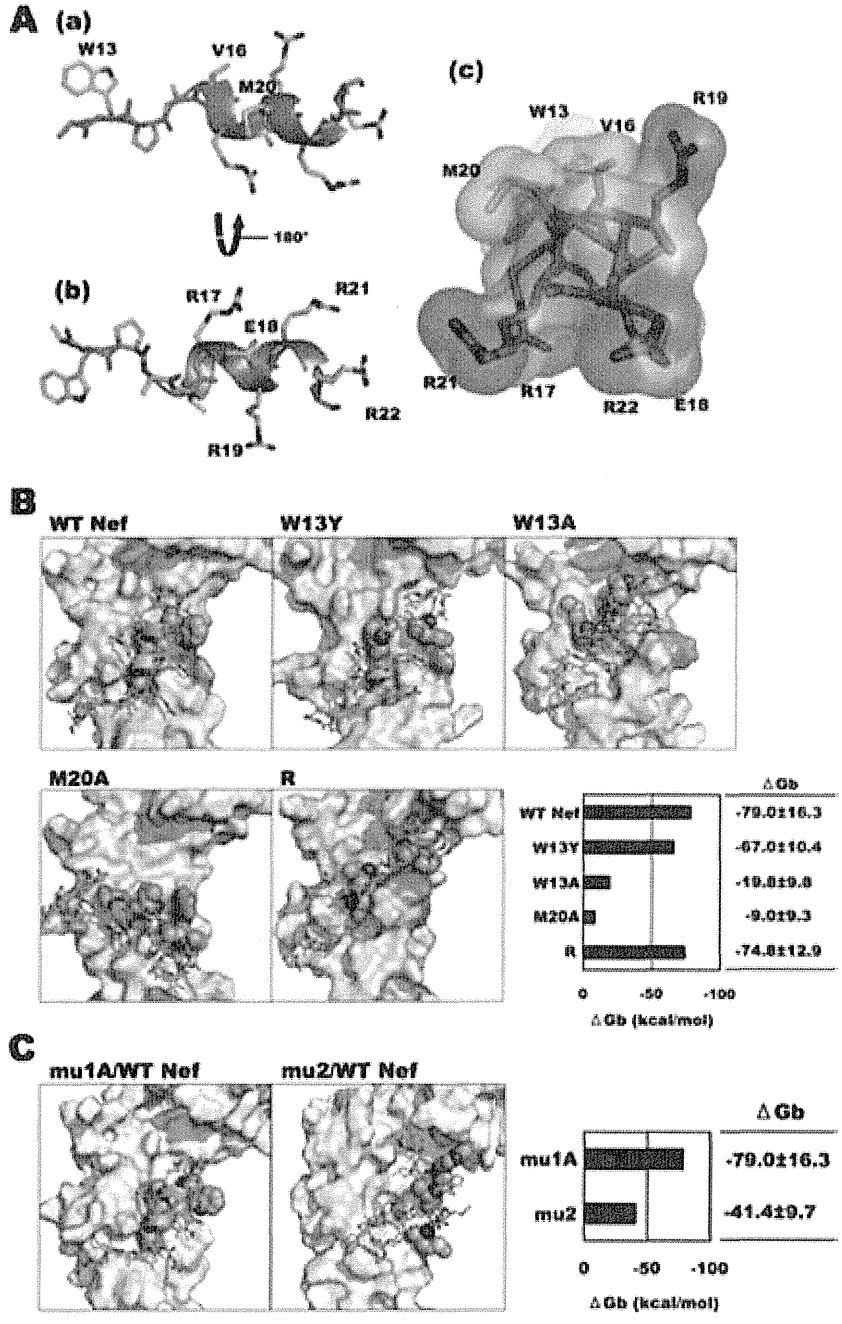

FIG 3 The three amino acids may form the site of binding to mu-1A, as shown by simulation *in silico*. (A) Molecular structure showing residues 13 to 23 of Nef taken from the NMR structure of myristoylated HIV-1 Nef residues 1 to 56 (PDB code 1QA5). Atoms are indicated as follows: red, oxygen atoms; blue, nitrogen atoms; green, carbon atoms; yellow, sulfur atoms; gray, main chain atoms (N, Cα, C, O). The helix conformation is indicated by ribbon representations. (a) and (b) represent side views rotated 180°. (c) illustrates a front view obtained by rotating (a) 90° around its short axis. (B) Final structures of each MD simulation. Atoms of mu-1A are represented by white surfaces, and atoms of Nef are shown in green. The 13th, 16th, and 20th amino acids in the Nef are highlighted with sphere representations. The Phe18 and Trp240 in mu-1A are highlighted in orange. Calculated binding energies between mu-1A and Nef mutants are indicated. (C) Summary of binding mode of mu-1A or mu-2 with WT Nef and calculated binding energies between mu-1A/mu-2 and Nef mutants.

to Met20, the Trp13 and Val16 residues in Nef were critical for the MHC-I downregulation.

The significance of the tripartite residues for MHC-I downregulation. In order to get insights into the structural properties of the tripartite Trp13, Val16, and Met20 (WVM) motif in Nef, we projected our results onto the NMR structure of the myristoylated Nef N terminus (PDB entry 1QA5) (15). Residues Val16 and Met20 were located on the same side of the N-terminal α-helix of Nef. In contrast, Arg17, -19, -21, and -22 residues were located on the opposite side of the α-helix, thus creating a basic surface. Trp13 was positioned immediately upstream of the N-terminal helix, with its hydrophobic side chain pointing in the same direction as those of Val16 and Met20 (Fig. 3A). Together, Trp13, Val16, and Met20 formed a hydrophobic surface of about 375 Å^2.

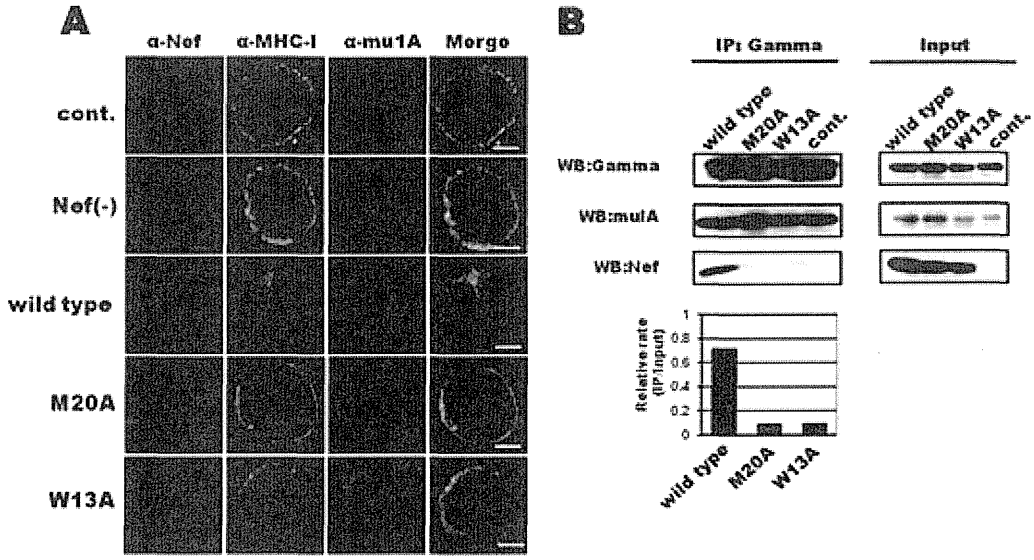

FIG 4 Two amino acids at the N terminus of Nef contribute to binding with mu-1A. (A) Immunofluorescence staining. Cells were stained with Nef, MHC-I, and mu-1A antibodies and analyzed by confocal microscopy. Blue, Nef; green, MHC-I; red, mu-1A. Bars, 10 μm. (B) Analysis of interaction of Nef proteins with mu-1A by coimmunoprecipitation. Jurkat cells infected with viruses were lysed at 24 h after infection and immunoprecipitated with an anti-gamma-adaptin MAb. The samples were detected by Western blotting using Nef and mu-1A antibodies. Immunoprecipitated samples of uninfected cells are shown as controls. Input controls were 1/50 of the volume of the immunoprecipitated protein.

These results may explain why the basic cluster adjacent to the Met20 comprised of Arg17, -19, -21, and -22 is dispensable for MHC-1 downregulation.

The mu-1A subunit of AP-1 has been shown to recognize binding motifs in the cytoplasmic tail of cargo proteins and binds them with the binding pockets. One of sorting motifs is an acidic dileucine motif (ED]xxxL[L), and the other is a tyrosine motif (YxxΦ; Φ represents bulky hydrophobic amino acids, which can be phenylalanine, isoleucine, leucine, methionine, or valine) (6a). Considering our finding that the replacement of Trp13 by Tyr but not Ala maintained the Nef effect on MHC-1 downregulation (Fig. 2), we hypothesized that Trp13 and Val16 could act as a noncanonical mu-1A-binding motif. To test this, we undertook docking simulations in terms of the interaction between the tyrosine motif-binding site of the mu-1A subunit and the N-terminal region of Nef. Based on the NMR structures of these proteins, we simulated the docking of the N-terminal region of Nef with mu-1A (Fig. 3B). An aromatic ring of the Trp13 of WT Nef was specifically placed in the front face of two aromatic rings of Phe18 and/or Trp 240 in mu-1A, contributing to hydrophobic interactions with the Nef N-terminal region. Protruding side chains of Met20 and Val16 of WT Nef were specifically embedded in a bowl shape of the hydrophobic cavity in the binding surface of mu-1A. In contrast, side chains of Arg17, -19, -21, and -22 residues were positioned in the direction opposite the mu-1A-binding surface. In addition, these hydrophobic interactions were well preserved in W13Y and R but not in W13A and M20A. Consequently, the binding configurations of these molecules were similar in the WT, W13Y, and R but not in W13A and M20A (Fig. 3B).

We then evaluated the influence of mutations on the binding free energy, ΔG_b, which indicates the binding strength between Nef and mu1A (Fig. 3B). The ΔG_bs of W13Y and the R mutant were nearly equal to that of the WT, whereas those of W13A and M20A were much lower, consistent with interaction modes of these variants in the structural models. These structural data were consistent with the results from the functional analyses presented in Fig. 2 and support our hypothesis that Trp13 and Val16 can form a noncanonical mu-1A-binding motif. Of note, the results from the interaction model showed that the hydrophobic motif of the WT Nef fitted only poorly onto mu-2, the subunit of AP-2, because of a poor fit of Met20 onto the mu-2-binding surface. Consequently, the ΔG_b between the N-terminal region of Nef and mu-2 was much lower than that of Nef and mu-1A (Fig. 3C). These results may explain why Met20 is critical for the selective binding of Nef to mu-1A, and the result is consistent with our finding that the N terminus of Nef is important for the downregulation of MHC-I but not of CD4.

The results of the computer simulation strongly suggest that the tripartite WVM motif contributes to the interaction of Nef with mu-1A. We further analyzed the intracellular localization in order to ascertain results from the docking simulation analyses. Immunofluorescence staining demonstrated that WT Nef but not M20A or W13A significantly colocalized with MHC-I and mu-1A and reduced the surface expression of MHC-I (Fig. 4A). Moreover, we sought to confirm the interaction of Nef with mu-1A by coimmunoprecipitation (Fig. 4B). Comparable levels of gamma and mu-1A subunits of the adapter complex as well as Nef were detected among the samples harvested from the Jurkat cells expressing WT Nef and its variants. Importantly, an anti-gamma adaptin antibody coprecipitated mu-1A irrespective of the expression of Nef due to the formation of a hemicomplex as subunits of AP-1, and the antibody also coprecipitated WT Nef but not the M20A and W13A mutants.

DISCUSSION

In the present study, we addressed the question of how the amino acids in the N terminus of Nef functioned for MHC-I downregu-

lation. We show here for the first time that Nef specifically interacts with the mu-1A subunit of AP-1 through the WVM domain and that Trp13 and Val16, in addition to Met20, are involved as a novel motif, which was evident from the present data obtained from functional, biochemical, structural, and *in silico* analyses.

We show here that the hydrophobic motif composed of Trp13, Val16, and Met20 interacts with mu-1A at the tyrosine motif-binding site. It is notable that Trp13 is highly conserved among HIV-1 subtypes whereas Val16 and Met20 are not necessarily conserved and V16I and M20I substitutions are also observed. In accordance with this point of view, we constructed structural models of mu-1A docked to the Nef N-terminal peptides containing a W13F, W13K, W13I, V16I, or M20I substitution. The models suggest that these peptides exert binding configurations comparable to that of wild-type Nef peptide, except for M20I, which appears to exhibit a substantial influence compared with the others (data not shown). Importantly, HIV-1 subtype C and simian immunodeficiency virus cpz (SIVcpz) Nef clones with the M20I substitution have been demonstrated to be functional in terms of the ability to downregulate MHC-I (18, 43, 46). Taken together, our results indicate that the hydrophobic patch interacts with mu-1A at the YXXΦ-binding site in a noncanonical manner and that the substitutions may not affect the MHC-I-regulatory function, which in turn implies that the highly conserved Trp13 could play a critical role for another function in Nef. These issues remain to be further elucidated.

The unique positioning of Met20 in the tripartite hydrophobic motif compared with the canonical tyrosine motif indicates that it is a critical residue to compensate for the absence of Tyr at position 13 and to selectively interact with mu-1A. Consistent with this notion, mu-2 showed much lower free binding energy than mu-1A due to the absence of an appropriate pocket structure such as is required for the interaction with the side chain of Met20 (Fig. 3C). It has been reported that Nef downregulates both MHC-I and CD4 through interaction with AP-1 and AP-2, respectively, and that a dileucine motif and a diacidic motif in the C terminus of Nef interact with the mu-2 subunit of AP-2 (12), while the molecular basis for the selective interaction of Nef with AP-1 and AP-2 remains to be elucidated. The present data showing that the hydrophobic motif in the N terminus of Nef specifically interacts with mu-1A of AP-1 explain the molecular mechanism for the differential effects of Nef on MHC-I and CD4.

Collins's group demonstrated that M20 was critical for the association of Nef with mu-1 as well as MHC-I downregulation (40, 49), which is consistent with our present results. In contrast, Singh et al. indicated in their report that M20 had little or no effect on the binding of Nef with mu-1 (42). This discrepancy may be due to differences in the assay systems used for detection of binding of Nef and mu-1, i.e., we as well as Collins's group employed T lymphocytes expressing Nef in a coimmunoprecipitation study as well as an MHC-I downregulation assay, whereas Singh et al. used an MHC-I-CD-Nef chimera and mu-1 expressed in *Escherichia coli* in an *in vitro* binding assay. We believe that the former approach should better represent the physiological machinery by which Nef exerts intrinsic activity.

In this study, we have found that the N-terminal region around the Met20 residue in Nef includes two separable functional motifs: an Arg-rich basic cluster and a noncanonical mu-1A-binding motif. Albeit overlapping in the primary structure, the two motifs were separable on the 3D structure of this region, as shown in Fig. 3. Previous reports have shown that the basic cluster supports plasma membrane binding of the myristoylated protein, including Src, MARCKS, and HIV-1 Gag, by contributing electrostatic interactions with negatively charged acidic phospholipids such as phosphatidylserine and phosphatidylinositol at the cytosolic surface of the plasma membrane (38) and also that the *N*-myristoylation is essential for the Nef-mediated biological activities, including MHC-I downregulation (2). We therefore hypothesized that Met20, together with the basic cluster, could play a critical role for the MHC-I downregulation. However, contrary to our assumption, the basic cluster was dispensable for the ability of Nef to downregulate MHC-I (Fig. 1), suggesting that that ability is independent of the association of Nef with phospholipids. Since Nef protein tends to localize to both the plasma membrane and perinuclear compartment (13), it is still possible that the myristoyl moiety could contribute to the MHC-I downregulation by way of association with the TGN or endosomes. This is in agreement with a previous report showing that the assembly of a complex that includes Nef, MHC-I, and AP-1 early in the secretory pathway is important for the MHC-I downregulation (20).

ACKNOWLEDGMENTS

We thank Hans-Georg Kräusslich (University of Heidelberg, Heidelberg, Germany) for the kind gift of pNL4-3Δmyr and R mutants, John C. Guatelli (University of California, San Diego) for the pNL4-3Δ62-68 plasmid, and Aikichi Iwamoto (University of Tokyo, Tokyo, Japan) for AIDS-patient sera. We also thank Hirofumi Okano, Tatsuya Harigae, and Terue Kurosawa for technical assistance.

This work was supported by grants-in-aid from the Ministry of Health, Labor and Welfare. S.I. was supported by a postdoctoral fellowship from the Japan Health Sciences Foundation.

REFERENCES

1. **Adachi A, et al.** 1986. Production of acquired immunodeficiency syndrome-associated retrovirus in human and nonhuman cells transfected with an infectious molecular clone. J. Virol. 59:284–291.
2. **Akari H, et al.** 2000. Nef-induced major histocompatibility complex class I down-regulation is functionally dissociated from its virion incorporation, enhancement of viral infectivity, and CD4 down-regulation. J. Virol. 74:2907–2912.
3. **Akari H, et al.** 1999. Pseudotyping human immunodeficiency virus type 1 by vesicular stomatitis virus G protein does not reduce the cell-dependent requirement of vif for optimal infectivity: functional difference between Vif and Nef. J. Gen. Virol. 80:2945–2949.
4. **Arhel NJ, Kirchhoff F.** 2009. Implications of Nef: host cell interactions in viral persistence and progression to AIDS. Curr. Top. Microbiol. Immunol. 339:147–175.
5. **Baugh LL, Garcia JV, Foster JL.** 2008. Functional characterization of the human immunodeficiency virus type 1 Nef acidic domain. J. Virol. 82: 9657–9667.
6. **Bentham M, Mazaleyrat S, Harris M.** 2006. Role of myristoylation and N-terminal basic residues in membrane association of the human immunodeficiency virus type 1 Nef protein. J. Gen. Virol. 87:563–571.

6a. **Bonifacino JS, Traub LM.** 2003. Signals for sorting of transmembrane proteins to endosomes and lysosomes. Annu. Rev. Biochem. 72:395–447.

7. **Bour S, Strebel K.** 1996. The human immunodeficiency virus (HIV) type 2 envelope protein is a functional complement to HIV type 1 Vpu that enhances particle release of heterologous retroviruses. J. Virol. 70:8285–8300.
8. **Chen R, Yokoyama M, Sato H, Reilly C, Mansky LM.** 2005. Human immunodeficiency virus mutagenesis during antiviral therapy: impact of drug-resistant reverse transcriptase and nucleoside and nonnucleoside reverse transcriptase inhibitors on human immunodeficiency virus type 1 mutation frequencies. J. Virol. 79:12045–12057.
9. **Collins KL, Chen BK, Kalams SA, Walker BD, Baltimore D.** 1998. HIV-1 Nef protein protects infected primary cells against killing by cytotoxic T lymphocytes. Nature 391:397–401.

10. **Crump CM, et al.** 2001. PACS-1 binding to adaptors is required for acidic cluster motif-mediated protein traffic. EMBO J. 20:2191–2201.
11. **Fölsch H, Ohno H, Bonifacino JS, Mellman I.** 1999. A novel clathrin adaptor complex mediates basolateral targeting in polarized epithelial cells. Cell 99:189–198.
12. **Foster JL, Denial SJ, Temple BR, Garcia JV.** 2011. Mechanisms of HIV-1 Nef function and intracellular signaling. J. Neuroimmune Pharmacol. 6:230–246.
13. **Gerlach H, et al.** 2010. HIV-1 Nef membrane association depends on charge, curvature, composition and sequence. Nat. Chem. Biol. 6:46–53.
14. **Gervaix A, et al.** 1997. A new reporter cell line to monitor HIV infection and drug susceptibility in vitro. Proc. Natl. Acad. Sci. U. S. A. 94:4653–4658.
15. **Geyer M, Munte CE, Schorr J, Kellner R, Kalbitzer HR.** 1999. Structure of the anchor-domain of myristoylated and non-myristoylated HIV-1 Nef protein. J. Mol. Biol. 289:123–138.
16. **Goto J, Kataoka R, Muta H, Hirayama N.** 2008. ASEDock-docking based on alpha spheres and excluded volumes. J. Chem. Inf. Model. 48:583–590.
17. **Greenberg ME, Iafrate AJ, Skowronski J.** 1998. The SH3 domain-binding surface and an acidic motif in HIV-1 Nef regulate trafficking of class I MHC complexes. EMBO J. 17:2777–2789.
18. **Heigele A, et al.** 2012. Down-modulation of CD8$\alpha\beta$ is a fundamental activity of primate lentiviral Nef proteins. J. Virol. 86:36–48.
19. **Hornak V, et al.** 2006. Comparison of multiple Amber force fields and development of improved protein backbone parameters. Proteins 65:712–725.
20. **Kasper MR, et al.** 2005. HIV-1 Nef disrupts antigen presentation early in the secretory pathway. J. Biol. Chem. 280:12840–12848.
21. **Kollman PA, et al.** 2000. Calculating structures and free energies of complex molecules: combining molecular mechanics and continuum models. Acc. Chem. Res. 33:889–897.
22. **Labute P.** 2008. The generalized Born/volume integral implicit solvent model: estimation of the free energy of hydration using London dispersion instead of atomic surface area. J. Comput. Chem. 29:1693–1698.
23. **Le Gall S, et al.** 1998. Nef interacts with the mu subunit of clathrin adaptor complexes and reveals a cryptic sorting signal in MHC I molecules. Immunity 8:483–495.
24. **Lubben NB, et al.** 2007. HIV-1 Nef-induced down-regulation of MHC class I requires AP-1 and clathrin but not PACS-1 and is impeded by AP-2. Mol. Biol. Cell 18:3351–3365.
25. **Luo R, David L, Gilson MK.** 2002. Accelerated Poisson-Boltzmann calculations for static and dynamic systems. J. Comput. Chem. 23:1244–1253.
26. **Lüthy R, Bowie JU, Eisenberg D.** 1992. Assessment of protein models with three-dimensional profiles. Nature 356:83–85.
27. **Mangasarian A, Piguet V, Wang JK, Chen YL, Trono D.** 1999. Nef-induced CD4 and major histocompatibility complex class I (MHC-I) down-regulation are governed by distinct determinants: N-terminal alpha helix and proline repeat of Nef selectively regulate MHC-I trafficking. J. Virol. 73:1964–1973.
28. **Meyer C, et al.** 2000. mu1A-adaptin-deficient mice: lethality, loss of AP-1 binding and rerouting of mannose 6-phosphate receptors. EMBO J. 19:2193–2203.
29. **Noviello CM, Benichou S, Guatelli JC.** 2008. Cooperative binding of the class I major histocompatibility complex cytoplasmic domain and human immunodeficiency virus type 1 Nef to the endosomal AP-1 complex via its mu subunit. J. Virol. 82:1249–1258.
30. **O'Doherty U, Swiggard WJ, Malim MH.** 2000. Human immunodeficiency virus type 1 spinoculation enhances infection through virus binding. J. Virol. 74:10074–10080.
31. **Onufriev A, Bashford D, Case DA.** 2004. Exploring protein native states and large-scale conformational changes with a modified generalized Born model. Proteins 55:383–394.
32. **Owen DJ, Evans PR.** 1998. A structural explanation for the recognition of tyrosine-based endocytotic signals. Science 282:1327–1332.
33. **Owen DJ, Setiadi H, Evans PR, McEver RP, Green SA.** 2001. A third specificity-determining site in mu 2 adaptin for sequences upstream of Yxx phi sorting motifs. Traffic 2:105–110.
34. **Page KA, Landau NR, Littman DR.** 1990. Construction and use of a human immunodeficiency virus vector for analysis of virus infectivity. J. Virol. 64:5270–5276.
35. **Pearlman DA, et al.** 1995. AMBER, a package of computer programs for applying molecular mechanics, normal mode analysis, molecular dynamics and free energy calculations to simulate the structural and energetic properties of molecules. Comput. Phys. Commun. 91:1–41.
36. **Peng B, Robert-Guroff M.** 2001. Deletion of N-terminal myristoylation site of HIV Nef abrogates both MHC-1 and CD4 down-regulation. Immunol. Lett. 78:195–200.
37. **Piguet V, et al.** 2000. HIV-1 Nef protein binds to the cellular protein PACS-1 to downregulate class I major histocompatibility complexes. Nat. Cell Biol. 2:163–167.
38. **Resh MD.** 1999. Fatty acylation of proteins: new insights into membrane targeting of myristoylated and palmitoylated proteins. Biochim. Biophys. Acta 1451:1–16.
39. **Riggs NL, Craig HM, Pandori MW, Guatelli JC.** 1999. The dileucine-based sorting motif in HIV-1 Nef is not required for down-regulation of class I MHC. Virology 258:203–207.
40. **Roeth JF, Williams M, Kasper MR, Filzen TM, Collins KL.** 2004. HIV-1 Nef disrupts MHC-I trafficking by recruiting AP-1 to the MHC-I cytoplasmic tail. J. Cell Biol. 167:903–913.
41. **Schwartz O, Marechal V, Le Gall S, Lemonnier F, Heard JM.** 1996. Endocytosis of major histocompatibility complex class I molecules is induced by the HIV-1 Nef protein. Nat. Med. 2:338–342.
42. **Singh RK, Lau D, Noviello CM, Ghosh P, Guatelli JC.** 2009. An MHC-I cytoplasmic domain/HIV-1 Nef fusion protein binds directly to the micro subunit of the AP-1 endosomal coat complex. PLoS One 4:e8364.
43. **Specht A, et al.** 2008. Selective downmodulation of HLA-A and -B by Nef alleles from different groups of primate lentiviruses. Virology 373:229–237.
44. **Tomiyama H, Akari H, Adachi A, Takiguchi M.** 2002. Different effects of Nef-mediated HLA class I down-regulation on human immunodeficiency virus type 1-specific CD8(+) T-cell cytolytic activity and cytokine production. J. Virol. 76:7535–7543.
45. **Tsodikov OV, Record MT, Jr, Sergeev YV.** 2002. Novel computer program for fast exact calculation of accessible and molecular surface areas and average surface curvature. J. Comput. Chem. 23:600–609.
46. **Turk G, et al.** 2009. Single Nef proteins from HIV type 1 subtypes C and F fail to upregulate invariant chain cell surface expression but are active for other functions. AIDS Res. Hum. Retroviruses 25:285–296.
47. **Wang J, Cieplak P, Kollman PA.** 2000. How well does a restrained electrostatic potential (RESP) model perform in calculating conformational energies of organic and biological molecules? J. Comput. Chem. 21:1049–1074.
48. **Welker R, Harris M, Cardel B, Krausslich HG.** 1998. Virion incorporation of human immunodeficiency virus type 1 Nef is mediated by a bipartite membrane-targeting signal: analysis of its role in enhancement of viral infectivity. J. Virol. 72:8833–8840.
49. **Wonderlich ER, Williams M, Collins KL.** 2008. The tyrosine binding pocket in the adaptor protein 1 (AP-1) mu1 subunit is necessary for Nef to recruit AP-1 to the major histocompatibility complex class I cytoplasmic tail. J. Biol. Chem. 283:3011–3022.
50. **Yang OO, et al.** 2002. Nef-mediated resistance of human immunodeficiency virus type 1 to antiviral cytotoxic T lymphocytes. J. Virol. 76:1626–1631.
51. **Yee JK, et al.** 1994. A general method for the generation of high-titer, pantropic retroviral vectors: highly efficient infection of primary hepatocytes. Proc. Natl. Acad. Sci. U. S. A. 91:9564–9568.

RESEARCH ARTICLE

VIROLOGY

Interferon-Induced SCYL2 Limits Release of HIV-1 by Triggering PP2A-Mediated Dephosphorylation of the Viral Protein Vpu

Kei Miyakawa,[1,2] Tatsuya Sawasaki,[3] Satoko Matsunaga,[1] Andrey Tokarev,[4] Gary Quinn,[1] Hirokazu Kimura,[5] Masako Nomaguchi,[6] Akio Adachi,[6] Naoki Yamamoto,[7] John Guatelli,[4,8] Akihide Ryo[1]*

Human cells respond to infection by retroviruses through the actions of proteins that inhibit the spread of viruses to other cells. One example is bone marrow stromal cell antigen 2 (BST2; also known as tetherin), which is an interferon (IFN)–inducible protein that restricts the release of progeny virions from infected cells. The HIV-1 accessory protein Vpu (viral protein U) causes degradation of BST2, and phosphorylation of Vpu at residues Ser^{52} and Ser^{56} is required for this function. We report that the host protein SCY1-like protein 2 (SCYL2) mediates the dephosphorylation of Vpu, antagonizing Vpu function and facilitating BST2-dependent restriction of HIV-1 release. SCYL2 reduced the number of virus particles released from cells infected with wild-type HIV-1, but not a strain lacking *vpu*, in a BST2-dependent manner. SCYL2 stimulated the dephosphorylation of Vpu on Ser^{52} and Ser^{56} by recruiting protein phosphatase 2A (PP2A) to Vpu. Conversely, depletion of SCYL2 resulted in enhanced phosphorylation of Vpu and increased viral particle release. Moreover, SCYL2 was produced in response to type I IFN and contributed to IFN-mediated viral restriction. Together, these results suggest that SCYL2 serves as a regulatory factor for Vpu, reducing the extent of Vpu phosphorylation and consequently enhancing BST2-mediated viral restriction.

INTRODUCTION

Accumulating evidence indicates that the HIV-1 accessory proteins antagonize host defenses to support efficient viral replication (*1–5*). Viral protein U (Vpu) is an 81–amino acid residue accessory protein that is encoded by HIV-1, simian immunodeficiency virus isolated from chimpanzees (SIV_{CPZ}), and some SIVs isolated from Old World monkeys (the SIV_{GSN} lineage). Vpu is translated from a bicistronic mRNA that also encodes the viral envelope glycoprotein (Env) (*6–8*). Although Vpu is not absolutely required for HIV-1 replication (*6*), studies with molecular clones of virus lacking *vpu* have demonstrated that the Vpu protein substantially enhances the production of infectious virus through at least two distinct mechanisms: the proteasomal degradation of CD4 (*9*) and the functional inactivation of the interferon (IFN)–inducible restriction factor bone marrow stromal cell antigen 2 (BST2; also known as tetherin) (*10*, *11*).

Cell-surface CD4 acts as an entry receptor for HIV-1, but it also inhibits its viral release and virion infectivity (*12*, *13*). CD4 binds to the Env precursor protein gp160 in the endoplasmic reticulum (ER) and inhibits its processing to gp120 and gp41. Vpu physically interacts with CD4 in the ER and facilitates its degradation, enabling Env processing and the efficient production of infectious virions (*14*). The restriction factor BST2 inhibits viral particle release, but similar to the effects of CD4, this inhibition is functionally counteracted by Vpu (*10*, *11*). Vpu reduces the cell-surface abundance of BST2 through transmembrane interactions (*11*, *15–21*), and it directs the degradation of BST2, primarily in lysosomes (*15–17*, *22–25*). In the absence of Vpu, BST2 cross-links nascent virions to the plasma membrane of infected cells and substantially inhibits the release of viral particles (*26–28*).

Previous reports indicated that Vpu is phosphorylated, presumably by casein kinase II (CKII), on two phospho-acceptor sites (Ser^{52} and Ser^{56}) in its cytoplasmic domain (*29*, *30*). Phosphorylation of both residues is required for efficient Vpu-mediated removal of BST2 from the cell surface as well as for the degradation of CD4 (*15*, *23*, *24*, *31*, *32*). The amino acid sequence of the region of Vpu ($DpS^{52}GxxpS^{56}$) that contains both phosphorylated serines (pS) residues is recognized by an F-box–containing ubiquitin ligase subunit, β transducin repeat–containing protein (β-TrCP). Vpu thus recruits the multisubunit SCF (Skp1-Cullin-F-box)–β-TrCP E3 ubiquitin ligase complex, which leads to the ubiquitination and degradation of BST2 and CD4 (*15*, *23*, *24*, *33*). Indeed, an HIV-1 clone carrying a mutation in the β-TrCP–binding motif of Vpu fails to reduce BST2 abundance in infected T cells (*15*, *34*). Although the phosphorylation of Vpu on Ser^{52} and Ser^{56} is a crucial step in the Vpu-dependent inhibition of BST2, how this process is further regulated is not well understood.

The type I IFN system, which includes IFN-α and IFN-β, is an innate immune response to viral infection and creates an antiviral state in cells that provides an important first line of defense against viral infection (*35*). Type I IFN is widely believed to have an inhibitory effect on HIV-1 replication (*36*). The biological response to IFN is mediated by its binding to the IFN receptors and the activation of the Janus-activated kinase (JAK)–signal transducer and activator of transcription (STAT) pathway, which leads to the expression of several hundred IFN-stimulated genes (ISGs) (*37*). Although BST2 has been described as an ISG (*38*), Vpu targets

[1]Department of Microbiology, Yokohama City University School of Medicine, Kanagawa 236-0004, Japan. [2]Japanese Foundation for AIDS Prevention, Tokyo 101-0061, Japan. [3]Cell-Free Science and Technology Research Center, Ehime University, Ehime 790-8577, Japan. [4]Department of Medicine, University of California, La Jolla, CA 92093, USA. [5]Infectious Disease Surveillance Center, National Institute of Infectious Diseases, Tokyo 208-0011, Japan. [6]Department of Microbiology, Institute of Health Biosciences, The University of Tokushima Graduate School, Tokushima 770-8503, Japan. [7]Department of Microbiology, National University of Singapore, Singapore 117597, Singapore. [8]San Diego Veterans Affairs Healthcare System, San Diego, CA 92161, USA.
*To whom correspondence should be addressed. E-mail: aryo@yokohama-cu.ac.jp

IFN-induced BST2 for removal from the cell surface, which is the apparent site of action of BST2 as a restriction factor. This suggests that Vpu plays a major role in conferring resistance on the innate immune response. However, treatment of HIV-1–infected cells with type I IFN can suppress viral particle release even in the presence of Vpu (*39–41*). This finding prompted us to hypothesize that the function of Vpu could be modulated by other host factors that would likely be induced by type I IFN; however, no such factor has yet been identified. To identify host factors that regulate Vpu activity, we used an in vitro, high-throughput protein-protein interaction assay with full-length HIV-1 Vpu and host kinase–related proteins synthesized in the wheat cell-free protein production system. Here, we report that SCY1-like protein 2 (SCYL2) is a functional interactor of Vpu and that it inhibits Vpu function by promoting the dephosphorylation of Vpu by the phosphatase protein phosphatase 2A (PP2A).

RESULTS

SCYL2 is a Vpu-binding host protein

We initially conducted in vitro protein-protein interaction analysis with full-length HIV-1 Vpu and host proteins. Because Vpu phosphorylation is required for its function, we focused on human protein kinases and related proteins as potential Vpu regulators. We synthesized more than 400 host proteins with a wheat cell-free protein production system (*42*) and screened them for their association with Vpu with the amplified luminescent proximity homogeneous assay (AlphaScreen) (*43*, *44*) (Fig. 1, A and B, and fig. S1). When a relative light unit per cutoff ratio of ≥5000 was used as the threshold, we identified 13 host proteins as potential factors to interact with Vpu that had not been previously known to do so (Fig. 1C). Using gene ontology analysis, we eliminated nuclear proteins relevant to transcriptional regulation or meiosis, enabling us to focus on nine proteins for additional screening (Fig. 1C). To assess the roles of these host proteins in the context of viral replication, we conducted small interfering RNA (siRNA)–based functional analysis of virus particle production. We transfected HeLa cells (which express BST2 endogenously) with siRNAs targeting the nine selected host factors, and then we transfected the cells with an HIV-1 proviral plasmid (pNL4-3). Subsequent measurement of the concentrations of the HIV-1 capsid protein p24 in the culture media by enzyme-linked immunosorbent assay (ELISA) revealed that siRNA specific for SCYL2 caused a substantial increase in viral particle release (Fig. 1D). On the basis of this initial screening, we focused on SCYL2 as a previously uncharacterized Vpu-interacting factor for in-depth functional analysis.

SCYL2 inhibits the particle release of Vpu-positive HIV-1

We next investigated whether SCYL2 affected viral particle release in the presence or absence of either BST2 or Vpu. We transfected HeLa cells with a wild-type or a Vpu-deficient HIV-1 molecular clone (pNL4-3 or pNL4-3ΔVpu) together with a plasmid encoding SCYL2. Viral release assays revealed that in HeLa cells expressing endogenous BST2, the presence of SCYL2 inhibited the release of wild-type HIV-1 particles and increased the amounts of intracellular BST2 (Fig. 2, A and B). Moreover, in cells transfected with pNL4-3ΔVpu, SCYL2 affected neither viral release nor intracellular BST2 abundance (Fig. 2, A and B). We further confirmed that SCYL2 had no observable suppressive effect on viral release in BST2-knockdown HeLa cells (Fig. 2C) or in human embryonic kidney (HEK) 293T cells, which lack endogenous BST2 (Fig. 2D). Moreover, the targeted depletion of endogenous SCYL2 substantially enhanced the release of wild-type virus, but not of Vpu-deficient virus, from cells containing BST2 (Fig. 2, E to G). Together, these results suggested that SCYL2 inhibited the release of viral particles only in the presence of BST2 and Vpu.

SCYL2 inhibits the Vpu-induced reduction in BST2 abundance

Many reports have demonstrated that Vpu enhances viral release by removing BST2 from the cell surface (*11*, *15–20*). To examine whether SCYL2 affected this function of Vpu, we investigated the amounts of cell-surface

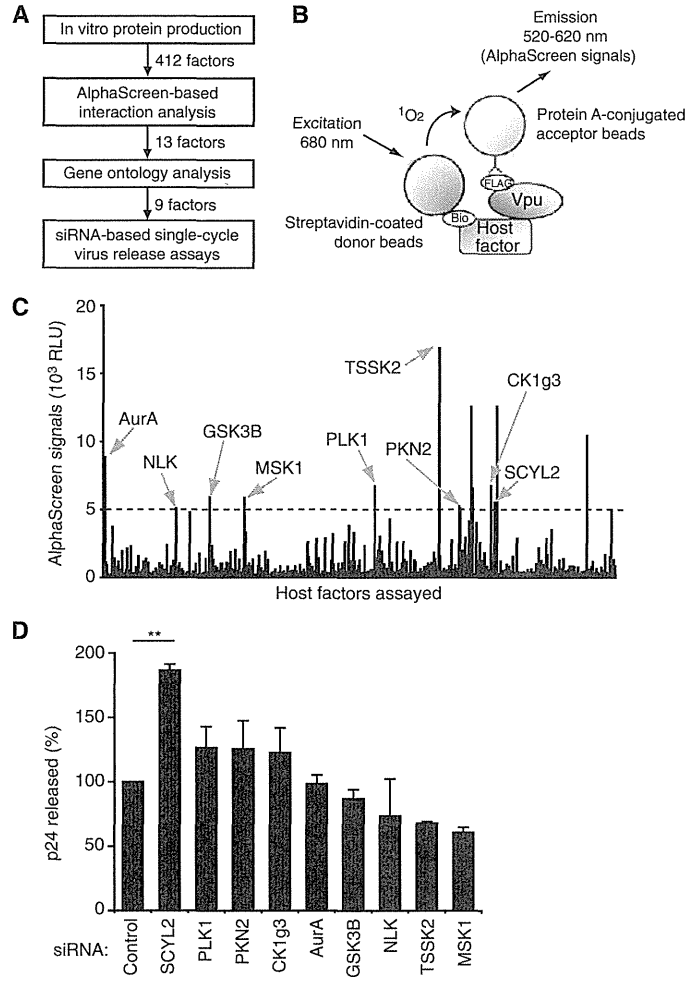

Fig. 1. SCYL2 is a Vpu-binding host protein. (A) Overview of the experimental procedure to detect regulatory factors for HIV-1 Vpu. (B) Schematic representation of the amplified luminescent proximity homogeneous assay used to identify Vpu-interacting proteins. Streptavidin-coated donor beads and anti-FLAG antibody conjugated to protein A acceptor beads were mixed with Vpu and human host proteins. If the two proteins are within 200 nm of each other, AlphaScreen signals are detected. (C) Thirteen proteins with high AlphaScreen signals were processed for further validation by gene ontology analysis. The nine kinases shown were selected as candidate Vpu-interacting host factors. The AlphaScreen was performed in duplicate for each sample. (D) An siRNA-based analysis measuring HIV-1 particle production. HeLa cells were treated with the indicated siRNAs for 24 hours before being transfected with the pNL4-3 molecular clone. Forty-eight hours after transfection, p24 protein in culture supernatants was measured by ELISA. $^{**}P = 0.0030$; $n = 3$ experiments.

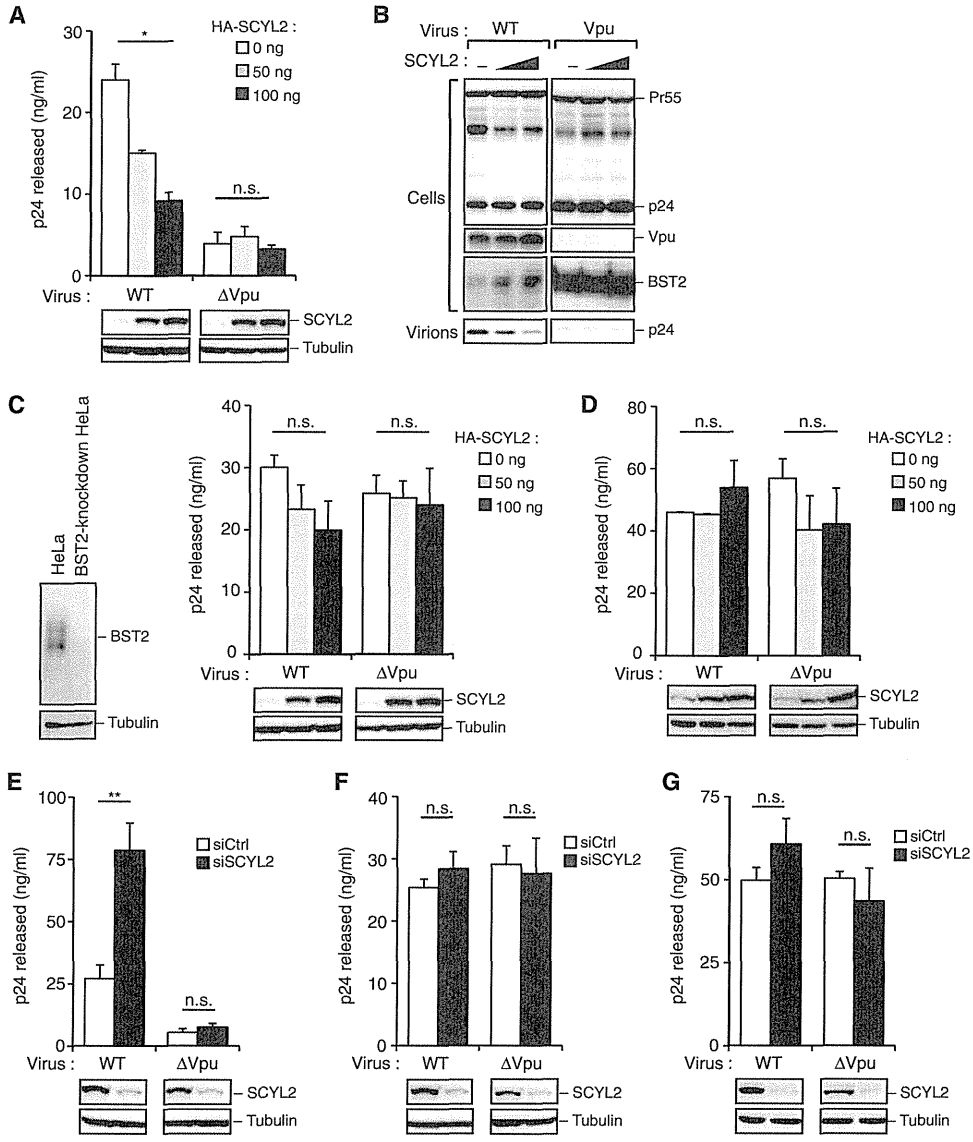

Fig. 2. SCYL2 inhibits the release of particles of Vpu-positive HIV-1. (A and B) Single-cycle virus release analysis of wild-type (WT) or Vpu-deficient HIV-1_{NL4-3}. HeLa cells were cotransfected with the indicated amounts of the SCYL2 expression plasmid together with 100 ng of either pNL4-3 (WT) or pNL4-3ΔVpu (ΔVpu). (A) Forty-eight hours after transfection, culture supernatants were analyzed by ELISA for p24 protein. Blots below the bar graph show the detection of SCYL2 and tubulin by Western blotting. n.s., not significant; *P = 0.0206; n = 3 experiments. (B) Cell lysates and supernatants were processed by Western blotting with antibodies against the indicated proteins. (C and D) SCYL2 fails to inhibit viral release from BST2-deficient cells. (C) BST2-knockdown HeLa cells and (D) HEK 293T cells (which have no endogenous BST2) were cotransfected with the indicated amounts of the SCYL2 expression plasmid together with 100 ng of either pNL4-3 or pNL4-3ΔVpu. Forty-eight hours after transfection, culture supernatants were analyzed by p24 ELISA. Western blotting analysis to detect BST2 abundance (C, left) and SCYL2 abundance (C and D, bottom) are shown. n.s., not significant; n = 3 experiments. (E to G) SCYL2 depletion enhances viral release from cells containing BST2. Single-cycle virus release analysis of WT or Vpu-deficient HIV-1_{NL4-3} in (E) HeLa cells, (F) BST2-knockdown HeLa cells, and (G) HEK 293T cells. Each cell type was treated with either control (white bars) or SCYL2-specific siRNAs (black bars) for 24 hours before being transfected with either pNL4-3 or pNL4-3ΔVpu (100 ng). Forty-eight hours after transfection, culture supernatants were analyzed by ELISA for p24. Western blotting analysis to detect endogenous SCYL2 abundance is shown at the bottom. n.s., not significant; **P = 0.0023; n = 3 experiments.

BST2 in HeLa cells expressing Vpu alone or in the presence of SCYL2. Consistent with previous studies, Vpu reduced the abundance of BST2 at the cell surface (Fig. 3A). However, this reduction was less apparent when cells were cotransfected with plasmids encoding both Vpu and SCYL2 (Fig. 3A). Western blotting analysis revealed that the presence of SCYL2 also inhibited the Vpu-mediated degradation of BST2 (Fig. 3B). We next addressed whether SCYL2 affected the anti-BST2 activity of Kaposi's sarcoma–associated herpesvirus (KSHV) K5 protein (*22*, *45*, *46*). Flow cytometric analysis demonstrated that SCYL2 was not able to revert the reduction in the cell-surface abundance of BST2 by KSHV K5 (Fig. 3C). Furthermore, SCYL2 inhibited the ability of Vpu to remove CD4 from the cell surface (Fig. 3D). These results indicated that SCYL2 specifically antagonized the function of Vpu and that this antagonism applied to the effects of Vpu on two cellular targets, CD4 and BST2.

SCYL2 inhibits the phosphorylation of Vpu on Ser^{52} and Ser^{56}

Vpu contains two conserved phosphoacceptor sites (Ser^{52} and Ser^{56}) in its cytoplasmic domain. Phosphorylation of these residues by CKII is required for efficient Vpu function with respect to decreasing the abundances of both BST2 and CD4 (*15*, *23*, *24*, *31*, *32*). We thus speculated that SCYL2 might affect the phosphorylation status of Vpu at Ser^{52} and Ser^{56}. To monitor the extent of Vpu phosphorylation in cells, we used phosphate-affinity polyacrylamide gel electrophoresis (Phos-tag PAGE) (*47*). This method enables the visualization of the phosphorylation status of a protein as a distinct band shift (*48*, *49*). In our Phos-tag PAGE analysis, wild-type Vpu was detected as an upper-shifted band, whereas a mutant Vpu in which Ser^{52} and Ser^{56} were replaced with alanines [Vpu(S52,56A)] was detected as a lower-shifted band, suggesting that the slower-migrating band was as a result of the phosphorylation of Vpu on Ser^{52} and Ser^{56} (Fig. 4A). SCYL2 converted wild-type Vpu into its dephosphorylated state (Fig. 4A). To confirm this observation, we generated a phospho-specific antibody against Ser^{52} and Ser^{56} of Vpu that detects wild-type Vpu but neither the Vpu(S52,56A) mutant nor calf intestinal phosphatase–treated wild-type Vpu (Fig. 4B). We used this antibody for Western blotting analysis and found, as expected, that SCYL2 reduced the extent

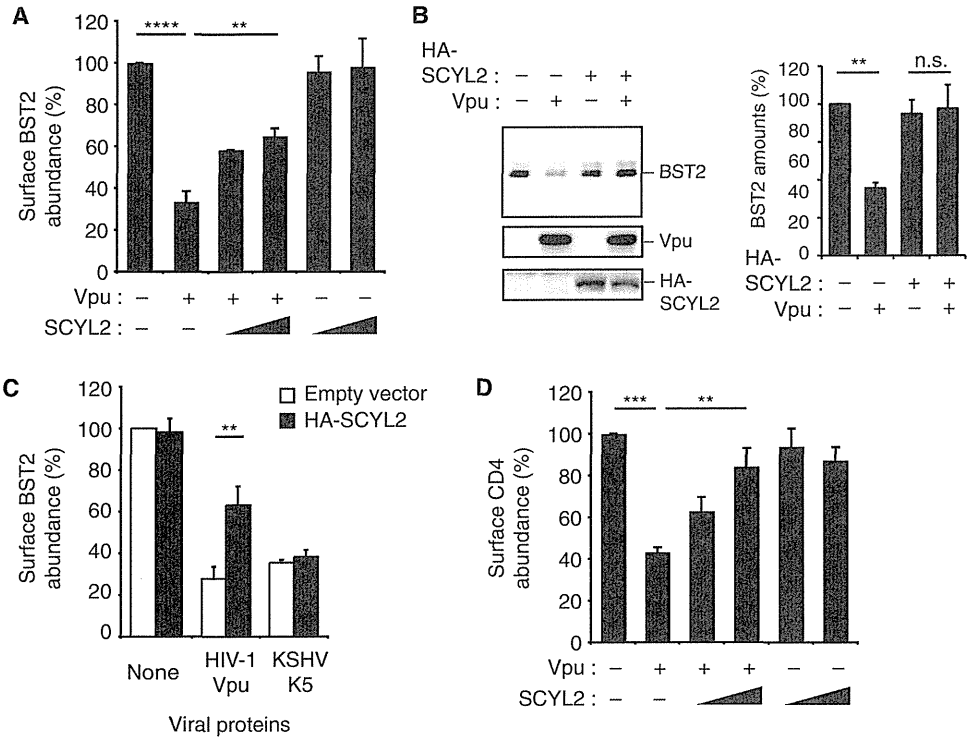

Fig. 3. SCYL2 inhibits the Vpu-induced reduction in BST2 abundance at the cell surface. (A) HeLa cells were transfected with combinations of plasmids encoding Vpu (0 and 100 ng) and hemagglutinin (HA)–SCYL2 (0, 500, and 1000 ng). The cell-surface abundance of BST2 was measured by flow cytometry. ****$P < 0.0001$; **$P = 0.0077$; $n = 3$ experiments. (B) HeLa cells were cotransfected with plasmids encoding Vpu and HA-SCYL2 at a molar ratio of 1:10. Cell lysates were processed for Western blotting analysis with anti-BST2, anti-Vpu, and anti-HA antibodies (left). Representative blots of three experiments are shown. The bar chart indicates the amounts of BST2 as determined by densitometric analysis of Western blots. n.s., not significant; **$P = 0.0020$; $n = 3$ experiments. (C) Selective inhibition of Vpu by SCYL2. HeLa cells were cotransfected with plasmid encoding HA-SCYL2 together with plasmids encoding the indicated viral proteins. After 18 hours, cell-surface BST2 abundance in the presence or absence of HA-SCYL2 was measured by flow cytometry. **$P = 0.0045$; $n = 3$ experiments. (D) SCYL2 inhibits the Vpu-induced down-regulation of CD4. H9 cells were transfected with combinations of plasmids encoding Vpu (0 and 100 ng) and HA-SCYL2 (0, 500, and 1000 ng). The cell-surface abundance of CD4 was quantified by flow cytometry. ***$P = 0.0002$; **$P = 0.0083$; $n = 3$ experiments.

of Vpu phosphorylation on Ser^{52} and Ser^{56} (Fig. 4C). Conversely, the targeted depletion of endogenous SCYL2 increased the amounts of phosphorylated Vpu (pVpu) (Fig. 4D). To confirm whether the effect of SCYL2 was mediated by dephosphorylation of Vpu, we treated cells with the CKII inhibitor DRB to suppress the phosphorylation of Vpu on Ser^{52} and Ser^{56}. Treatment with DRB decreased the extent of Vpu phosphorylation, and it inhibited the reduction of cell-surface BST2 abundance by Vpu (fig. S2). Together, these results suggested that SCYL2 inhibited Vpu phosphorylation on Ser^{52} and Ser^{56}, crucial residues for the function of Vpu in the reduction of BST2 abundance, as well as that of CD4.

Both the kinase-like domain and the clathrin-binding domain of SCYL2 are required for its anti-Vpu activity

To verify the association between Vpu and SCYL2 in cells, we next examined the intracellular localization of both proteins by immunofluorescence confocal microscopy. Our results indicated the colocalization of SCYL2 and Vpu in the perinuclear region and cytoplasm (Fig. 5A). We confirmed a direct interaction between SCYL2 and Vpu in vitro with glutathione *S*-transferase (GST) pull-down analysis, which showed that SCYL2 copurified with GST-tagged Vpu (Fig. 5B). We next attempted to determine the binding domain of SCYL2 responsible for its interaction with Vpu in experiments with several truncation mutants of SCYL2 (Fig. 5C). SCYL2 contains an N-terminal kinase-like domain (KLD) and a C-terminal clathrin-binding domain (CBD) (*50–52*). Immunoprecipitation analysis demonstrated that Vpu coprecipitated with either full-length SCYL2 or its two C-terminal truncation mutants, termed SCYL2(N) and SCYL2(ΔCBD), but not with the N-terminal truncation mutant SCYL2(ΔKLD) (Fig. 5C). These results indicated that Vpu interacted with the KLD of SCYL2. We next examined which portions of SCYL2 were important for the dephosphorylation of Vpu and for viral restriction. Our functional analysis demonstrated that SCYL2(ΔKLD) failed to inhibit the activity of Vpu, which was consistent with its inability to bind to Vpu (Fig. 5, D and E). SCYL2(N) and SCYL2(ΔCBD) were also unable to suppress the function of Vpu (Fig. 5, D and E), potentially as a result of their inability to bind to clathrin. These data suggested that both the KLD and CBD of SCYL2 were required for its function.

SCYL2 affects the transport of intracellular proteins through its role in clathrin-mediated membrane trafficking (*51*). The SCYL2 CBD is functionally indispensable because of its association with the clathrin heavy chain (CHC) and the consequent localization of SCYL2 to clathrin-coated vesicles (*51*). To investigate whether clathrin-dependent membrane traffic was necessary for the effects of SCYL2 on Vpu, we performed experiments with cells transfected with CHC-specific siRNA. SCYL2-mediated dephosphorylation of Vpu was inhibited in CHC-depleted cells compared to that in control cells (Fig. 5F). Immunofluorescence analysis further revealed that the depletion of CHC resulted in the diffuse cytoplasmic localization of SCYL2, consistent with a previous report (*51*), and the lack of colocalization of SCYL2 with Vpu (Fig. 5G). These results suggested that clathrin-mediated membrane trafficking is required for the function of SCYL2 as an inhibitor of Vpu.

To address whether the SCYL2-Vpu interaction might be conserved during viral evolution, we investigated the association of SCYL2 with SIV_{GSN} Vpu, an ancient predecessor of HIV-1 Vpu. Amino acid sequence alignment revealed that SIV_{GSN} Vpu lacked the phospho-acceptor sites that correspond to Ser^{52} and Ser^{56} in HIV-1 Vpu (fig. S3A). We found no observable interaction between SIV_{GSN} Vpu and SCYL2 (fig. S3B). Furthermore, cotransfection of cells with plasmids encoding SCYL2 and SIV_{GSN} Vpu did not revert the anti-BST2 activity of SIV_{GSN} Vpu, whereas SCYL2 antagonized the activity of HIV-1 Vpu (fig. S3, C and D). These

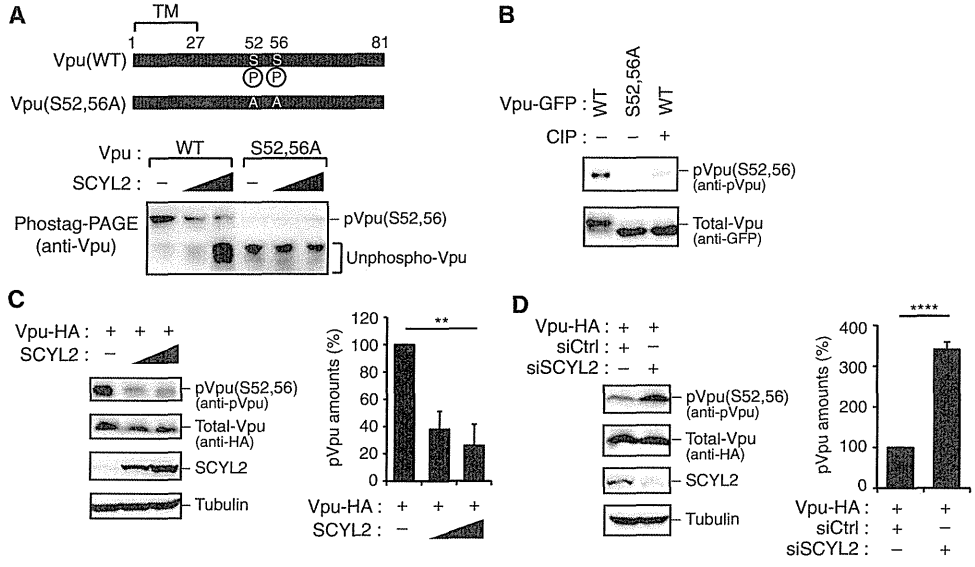

Fig. 4. SCYL2 inhibits the phosphorylation of Vpu on Ser^{52} and Ser^{56}. (A) Schematic representation of Vpu phosphorylated at Ser^{52} and Ser^{56} and of alanine substitution mutants at these sites. HEK 293T cells were cotransfected with plasmids encoding either WT Vpu or the Vpu(S52,56A) mutant (100 ng) together with the SCYL2 expression plasmid (at 0, 500, or 1000 ng). Forty-eight hours after transfection, cell lysates were subjected to Phos-tag PAGE analysis. Blots were incubated with anti-Vpu antibody. (B) Specific recognition of pVpu by an anti-pVpu($Ser^{52,56}$) antibody. HEK 293T cells were transfected with expression plasmids encoding GFP-tagged WT Vpu or the Vpu(S52,56A) mutant. Twenty-four hours after transfection, cell lysates were incubated with buffer alone or with calf intestinal alkaline phosphatase for 30 min before Western blotting analysis was performed with the indicated antibodies. (C) SCYL2 facilitates the dephosphorylation of Vpu on Ser^{52} and Ser^{56}. HEK 293T cells were transfected with plasmids encoding Vpu-HA and SCYL2 at a molar ratio of 1:5 or 1:10. Twenty-four hours after transfection, cell lysates were processed for Western blotting analysis with antibodies against the indicated proteins. The bar chart indicates the amounts of pVpu as determined by densitometric analysis of Western blots. $^{**}P = 0.0012$. (D) HEK 293T cells were treated with either control (siCtrl) or SCYL2-specific siRNA (siSCYL2) for 24 hours before being transfected with 100 ng of Vpu expression plasmids. Cell lysates were subjected to Western blotting analysis with antibodies against the indicated proteins. The bar chart indicates the amounts of pVpu as determined by densitometric analysis of Western blots. $^{****}P < 0.0001$. All data are from single experiments and are representative of three experiments.

data suggested that the interaction between SCYL2 and Vpu might have developed during the evolution of primate lentiviruses.

SCYL2 promotes PP2A-mediated dephosphorylation of Vpu

Our earlier results suggested that SCYL2 interacted with Vpu and inhibited its function by promoting the dephosphorylation of Vpu at residues Ser^{52} and Ser^{56}. To investigate the molecular mechanism underlying this process, we next addressed whether SCYL2 had phosphatase activity toward Ser^{52} and Ser^{56} on Vpu. To this end, we incubated SCYL2 immunoprecipitates with either phosphorylated or nonphosphorylated Vpu peptide containing Ser^{52} and Ser^{56} (AEDpS^{52}GNEpS^{56}EGE) and then measured the amounts of free phosphate released. We found that SCYL2 immunoprecipitates had phosphatase activity toward Ser^{52} and Ser^{56} on Vpu, which was blocked by a phosphatase inhibitor, okadaic acid (OA) (Fig. 6A). Furthermore, treatment of cells with OA blocked SCYL2-mediated dephosphorylation of Vpu and inhibition of viral release (Fig. 6, B and C). Because OA specifically inhibits the activity of PP2A in vivo, we next asked whether PP2A physically associated with SCYL2. The core structure of PP2A consists of a scaffold A subunit (PP2A/A) and a catalytic C subunit ($PP2A_C$) (*53*). Immunoprecipitation analysis revealed that SCYL2 specifically interacted with PP2A/A, but not with $PP2A_C$ (Fig. 6D), suggesting the possibility that SCYL2 recruits the scaffold subunit of PP2A to Vpu. As expected, in the presence of SCYL2, the interaction between Vpu and PP2A/A was enhanced (Fig. 6E). Moreover, Vpu interacted with endogenous SCYL2 and PP2A in HEK 293T cells (Fig. 6F). Depletion of PP2A/A by specific siRNA abrogated the SCYL2-mediated dephosphorylation of Vpu (Fig. 6G). Furthermore, immunofluorescence analysis revealed that SCYL2 induced the colocalization of PP2A/A with both Vpu and SCYL2 in the perinuclear region (Fig. 6H). These observations suggested that SCYL2 promoted Vpu dephosphorylation by recruiting PP2A to pVpu.

SCYL2 affects Vpu function through a phosphorylation-dependent mechanism

Several studies have suggested that the mechanism by which BST2 antagonizes Vpu function is partly independent of β-TrCP and BST2 degradation (and therefore partly independent of the phosphorylation of Ser^{52} and Ser^{56}) (*54*, *55*). We thus explored the possibility that SCYL2 might affect Vpu function through a phosphorylation-independent mechanism. To this end, we first investigated whether SCYL2 associated with the nonphosphorylated form of Vpu. Immunoprecipitation analysis demonstrated that both wild-type Vpu and the Vpu(S52,56A) mutant interacted with endogenous SCYL2 (fig. S4A). We next addressed whether SCYL2 interfered with the direct interaction between Vpu and BST2 and thereby inhibited viral release. Bimolecular fluorescence complementation analysis (*56*, *57*) revealed that SCYL2 did not interfere with the association of BST2 with either wild-type Vpu or the Vpu(S52,56A) mutant in live cells (fig. S4C). In contrast, viral release assays demonstrated that overexpression of SCYL2 inhibited the release of wild-type HIV-1 but not of its derivative encoding the Vpu(S52,56A) mutant (fig. S4, D and E). Together, these data suggested that SCYL2 interfered with the anti-BST2 activity of Vpu through a phosphorylation-dependent mechanism.

SCYL2 affects the type I IFN–mediated antiviral response

BST2 acts as a key effector of the type I IFN–inducible antiviral response (*58*). We thus investigated whether SCYL2 might also affect this response. We treated epithelial (HeLa) and $CD4^+$ T lymphocyte (H9) cell lines with type I IFN (that is, IFN-α and IFN-β) for 6 hours and then analyzed the expression of SCYL2 by reverse transcription polymerase chain reaction (RT-PCR) or Western blotting analysis. Type I IFN increased the abundance of SCYL2 mRNA and protein in both cell lines (Fig. 7A). Moreover, analysis of reporter gene expression revealed that the 5′ untranslated region of the gene encoding

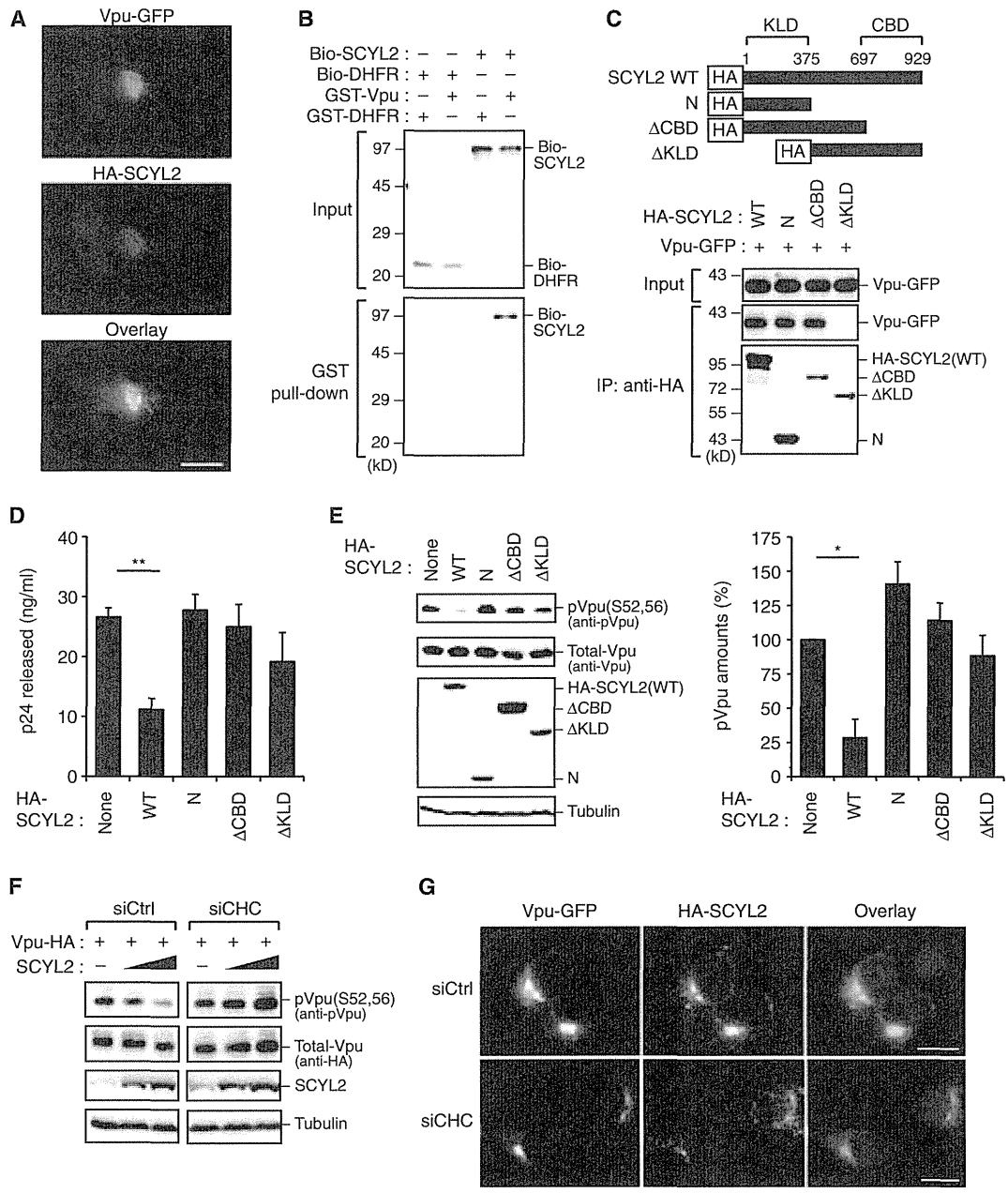

Fig. 5. Both the KLD and CBD of SCYL2 are required for its ability to antagonize Vpu activity. (A) Colocalization of Vpu and SCYL2 in cells. HeLa cells were transfected with plasmids encoding Vpu-GFP and HA-SCYL2. After 24 hours, the cells were fixed, permeabilized, and stained with anti-HA antibody (red), followed by confocal microscopic analysis. Nuclei were stained with 4′,6-diamidino-2-phenylindole (DAPI) and are shown in blue. Scale bar, 10 μm. (B) SCYL2 interacts with Vpu in vitro. Recombinant biotinylated SCYL2 (Bio-SCYL2) and biotinylated dihydrofolate reductase (Bio-DHFR) were processed for GST pull-down analysis with either GST-Vpu or GST-DHFR. DHFR was used as a negative control. Captured proteins were analyzed by Western blotting with streptavidin-HRP. (C) The N-terminal KLD of SCYL2 interacts with Vpu. HEK 293T cells were cotransfected with plasmids encoding Vpu-GFP together with plasmid encoding WT SCYL2 or one of its truncation mutants. Cell lysates were immunoprecipitated (IP) with anti-HA antibody and then analyzed by Western blotting with anti-GFP or anti-HA antibodies. (D and E) SCYL2 mutants lacking the CBD have no observable effect on (D) viral release or (E) Vpu dephosphorylation. Cells were cotransfected with pNL4-3 (100 ng) together with the indicated SCYL2 expression plasmids (100 ng). Forty-eight hours after transfection, culture supernatants and cell lysates were subjected to (D) p24 ELISA or (E) Western blotting analysis with anti-pVpu, anti-Vpu, anti-HA, and anti-tubulin antibodies. The bar chart in (E) indicates the amounts of pVpu as determined by densitometric analysis of Western blots. $^{**}P$ = 0.0045; $^{*}P$ = 0.0172; n = 3 experiments. (F) CHC depletion abrogates SCYL2-mediated dephosphorylation of Vpu. HEK 293T cells were treated with either control (siCtrl) or CHC-targeted siRNA (siCHC) for 24 hours before being transfected with plasmids expressing Vpu-HA and SCYL2 at a molar ratio of 1:5 or 1:10. Forty-eight hours after transfection, cell lysates were subjected to Western blotting with the indicated antibodies. (G) CHC depletion interferes with the colocalization of SCYL2 and Vpu. HeLa cells were treated with either control or CHC-specific siRNA for 24 hours before being transfected with plasmids encoding Vpu-GFP and HA-SCYL2. After 24 hours, the cells were fixed, permeabilized, stained with anti-HA antibody (red), and analyzed by confocal microscopy. Nuclei were stained with DAPI (blue). Scale bars, 10 μm. Data shown in (A) to (C) and (E) to (G) are representative of three experiments.

SCYL2 was transactivated by IFN-β (Fig. 7B). We next examined whether type I IFN promoted the SCYL2-mediated dephosphorylation of Vpu. To this end, we infected HeLa and H9 cells with vesicular stomatitis virus glycoprotein (VSVG)–pseudotyped HIV-1 and then treated the cells with IFN-β. As expected, the addition of IFN-β induced the dephosphorylation of Vpu (Fig. 7C). Single-cycle virus release analysis revealed that IFN-β decreased the amounts of virus released (Fig. 7D), as reported previously (*41*). However, the targeted depletion of SCYL2 by siRNA partially blocked IFN-β–mediated viral restriction (Fig. 7D). This was not the case in parallel experiments with Vpu-deficient viruses or BST2-deficient cells (Fig. 7, E and F). Together,